Journal of *Marine Science and Engineering*

MDPI

Review

Numerical Modelling of Scour Around Coastal and Offshore Infrastructure

Marios Koronides [1,*], Constantine Michailides [2] and Toula Onoufriou [1]

[1] Department of Civil Engineering and Geomatics, Cyprus University of Technology, 3036 Limassol, Cyprus; t.onoufriou@cut.ac.cy
[2] Department of Civil Engineering, International Hellenic University, 621 24 Serres, Greece; cmichailides@ihu.gr
* Correspondence: marios.koronides@cut.ac.cy

Abstract

Scour around coastal and offshore infrastructure is a critical concern, influencing foundation stability, structural performance, and long-term safety under wave–current loading. Reliable scour prediction is essential for designing resilient foundations for offshore wind turbines, bridge piers, subsea pipelines, breakwaters, and coastal protection systems. While physical modelling has advanced understanding of sediment entrainment and bed–flow interactions, numerical modelling is increasingly used to predict scour under complex, transient hydrodynamic conditions. This review provides a comprehensive assessment of the principal numerical approaches currently used to simulate scour. Four major modelling frameworks are examined: single-phase Eulerian Computational Fluid Dynamics (CFD), two-phase Eulerian–Eulerian CFD, coupled CFD–Discrete Element Method (CFD–DEM) approaches, and mesh-free Smoothed Particle Hydrodynamics (SPH) including SPH–DEM. For each method, governing formulations, sediment-transport models, turbulence closures, bed-evolution treatment, and fluid–sediment coupling procedures are critically evaluated. The review identifies the key strengths and limitations of each approach and assesses their suitability across different scour regimes. Remaining numerical challenges are highlighted, together with future research directions aimed at improving the reliability, robustness, and engineering applicability of scour modelling. The comparative assessment is structured around the core dimensions of underlying assumptions and physical representation, sediment-transport and bed-evolution capabilities, fluid–sediment coupling and process resolution, validation maturity, computational requirements and scalability, and engineering applicability.

Keywords: scour modelling; coastal and offshore infrastructure; CFD; CFD–DEM coupling; SPH; bed evolution; numerical modelling

Check for updates

Academic Editor: Giacomo Viccione

Received: 3 August 2026
Revised: 7 September 2026
Accepted: 18 September 2026
Published: 23 September 2026

Copyright: © 2026 by the authors. Licensee MDPI, Basel, Switzerland. This article is an open access article distributed under the terms and conditions of the Creative Commons Attribution (CC BY) license.

1. Introduction

Scouring refers to the removal and transport of sediment caused by the action of waves, currents, or their combined effects in the vicinity of a structure. It is recognised as one of the primary causes of foundation instability in marine and hydraulic engineering [1–4] as it directly alters soil resistance and the associated failure mechanisms [5–7]. Offshore wind turbines, bridge piers, subsea pipelines, and breakwaters are particularly susceptible, and failures associated with scour can result in costly repairs, operational downtime, or even structural collapse. Because these systems operate in highly dynamic marine geotechnical environments, reliable modelling of seabed–structure–hydrodynamic interaction is

essential. The mechanisms underlying scour development are complex and depend on an interplay between hydrodynamic loading, sediment properties, and structural geometry [8,9]. Scour is commonly described in terms of its spatial scale and the dominant driving forces. Local scour occurs immediately adjacent to the structure, where flow-energy gradients and vortex formation generate intense bed shear stresses that mobilise sediment. Global scour represents a more uniform lowering of the seabed profile over a large area, often due to broader changes in hydrodynamics or sediment supply [9].

Laboratory flume experiments have been instrumental in advancing the understanding of scour mechanisms [9–13]. Field monitoring has provided valuable insight into sediment mobilisation under wave forcing [14–16] and has been used as a basis for risk-mitigation strategies for scour hazards [17]. However, laboratory experiments are confined to small scales, where scaling-up can be challenging, and field-based studies remain relatively scarce and concentrated mainly on bridge-pier environments, with comparatively limited deployment for coastal or offshore infrastructure. Additionally, both laboratory and field observations are typically constrained by measurement limitations, often providing insufficient spatial and temporal resolution. Nevertheless, they remain essential for the calibration and validation of numerical models, which can subsequently provide high-resolution predictions with detailed representations of hydrodynamic and sediment-transport processes that cannot be captured through physical testing alone. Numerical models allow the isolation of individual processes, the testing of a wide range of environmental and structural conditions, and the simulation of extreme events that may be impractical to reproduce physically.

Advances in Computational Fluid Dynamics (CFD), multiphase flow modelling, and sediment-transport algorithms now make it possible to capture detailed hydrodynamic–sediment–structure interactions. Coupling hydrodynamic solvers with morphodynamic modules enables the simulation of evolving seabed topography, allowing for predictive studies of long-term scour development. The simulation of grain-scale scour mechanisms can be further enhanced by coupling CFD with the Discrete Element Method (DEM). In this approach, sediment particles and their contact interactions are explicitly represented, while fluid–particle interactions are transferred between the CFD and DEM frameworks through appropriate coupling formulations. Several reviews have addressed numerical local-scour modelling from different perspectives, including sediment-transport and CFD-based models [18], offshore wind-foundation scour [19,20], and broader local-scour prediction approaches [8]. Nevertheless, due to the diversity of available numerical approaches, there remains a need for a systematic cross-framework assessment of their underlying assumptions, validation maturity, computational requirements, and suitability for different engineering applications.

Accordingly, this review synthesises numerical approaches for scour modelling with emphasis on practical model selection and applicability to coastal and offshore infrastructure problems. In contrast to previous reviews with broader or application-specific scopes, the present study systematically compares single-phase Eulerian CFD, two-phase Eulerian–Eulerian CFD, CFD–DEM, and SPH/SPH–DEM as distinct modelling frameworks. The reviewed methods are evaluated in terms of their theoretical foundations, underlying assumptions, validation status, computational requirements, strengths, and limitations. A comparative synthesis is then used to identify the domains in which each method is most reliable, recognising that no single framework is equally appropriate for all scour regimes. Remaining numerical challenges and future research directions are also highlighted.

The review is therefore structured to support the selection of appropriate numerical frameworks for scour analysis in research and engineering applications involving coastal and offshore infrastructure. Section 2 provides an overview of the physical processes

governing scour, while Section 3 identifies the main modelling challenges in numerical scour analysis. Section 4 classifies the principal numerical approaches. Section 5 assesses finite-volume formulations, distinguishing between single-phase Eulerian and two-phase Eulerian–Eulerian CFD models. Section 6 reviews coupled CFD–Discrete Element Method (CFD–DEM) frameworks, while Section 7 examines mesh-free Smoothed Particle Hydrodynamics (SPH). After the individual methods are addressed, Section 8 presents a comparative synthesis across approaches. Section 9 outlines the remaining numerical challenges and identifies key research needs, and Section 10 provides concluding remarks.

2. Fundamentals of Scour Processes

The development of scour is fundamentally driven by the interaction between fluid flow, sediment transport, and structural geometry. When a flow encounters a structure, it is forced to change direction and accelerate around and down towards the bed, producing localised pressure gradients and strong vortical motions (Figure 1). At the upstream face, the downward deflection of the flow generates a horseshoe vortex that wraps around the base of the structure, enhancing the near-bed shear stresses and initiating sediment motion. Downstream, flow separation and reattachment lead to the formation of lee-wake vortices, which redistribute sediment and create zones of deposition. These coherent flow structures, documented in detail by Roulund et al. [11], can evolve dynamically in response to changes in bed morphology.

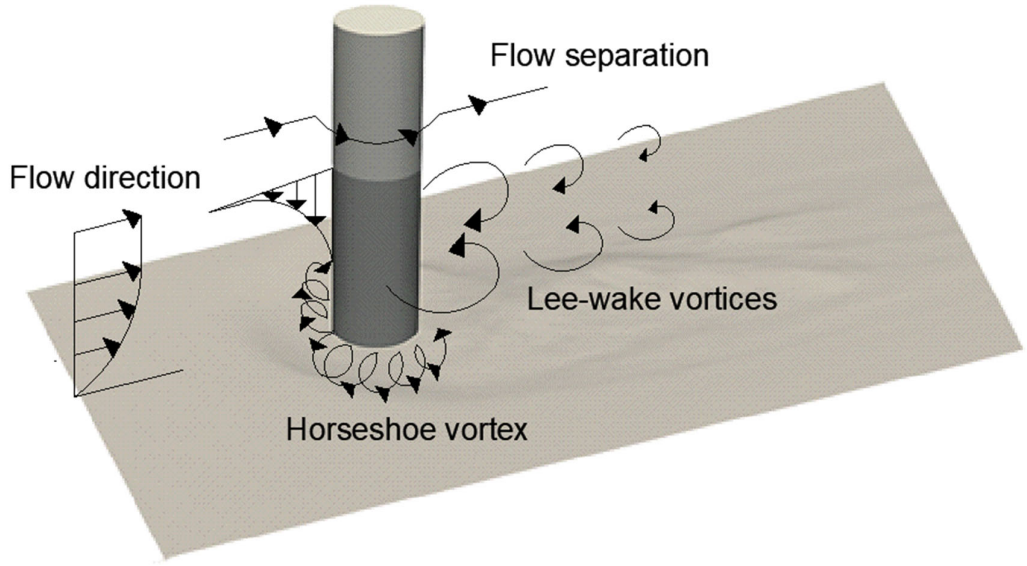


Figure 1. Schematic illustration of vortical motions and sediment scour and deposition.

Sediment transport can occur as bed shear stress increases above the critical threshold for sediment motion. At low excess shear, particles move as bed load through rolling, sliding, or saltation; with increasing shear, sediment becomes suspended by turbulent eddies. Under very energetic conditions, such as during storms or strong tidal currents, a sheet-flow regime may develop in which a continuous layer of sediment several grain diameters thick is mobilised above the static bed [21]. The transition between these transport regimes depends primarily on sediment mobility, turbulence and particle settling, and is influenced by parameters such as the Shields parameter and sediment properties.

Several dimensionless parameters are commonly used to characterise and predict scour processes. Among them, the Shields parameter θ (Equation (1)) provides a measure of the ratio between the driving fluid forces acting on sediment grains and the resisting gravitational forces, thereby indicating whether sediment motion will occur (i.e., when

$\theta > \theta_{cr}$). The critical Shields parameter $\theta_{cr,0}$ is defined by Equation (2) for a flat bed, while Equation (3) defines θ_{cr} that applies to a sloping bed [11,22,23]. An alternative approach is to retain $\theta_{cr,0}$ as the threshold and instead introduce an effective Shields parameter modified to incorporate the additional driving force induced by bed slope [24]. Beyond incipient motion, θ influences the rate of sediment transport through a power-law relationship, as discussed by Ma et al. [25] and Keetels et al. [26].

$$\theta = \frac{\tau}{g(\rho_s - \rho)d_{50}} \tag{1}$$

$$\theta_{cr,0} = \frac{\tau_{cr}}{g(\rho_s - \rho)d_{50}} = \frac{0.3}{1+1.2D_*} + 0.055\left(1 - e^{-0.02D_*}\right) \tag{2}$$

$$\theta_{cr} = \theta_{cr,0} \cdot \left(cos\beta \cdot \sqrt{1 - \frac{sin^2\alpha \cdot tan^2\beta}{tan^2\varphi}} - \frac{cos\alpha \cdot sin\beta}{tan\varphi} \right) \tag{3}$$

$$D_* = d_{50} \cdot \left(\frac{\left(\frac{\rho_s}{\rho} - 1\right) \cdot g}{\nu^2} \right)^{1/3} \tag{4}$$

where τ and τ_{cr} are the local and critical bed shear stresses, respectively, g is the gravitational acceleration, ρ_s is the sediment grain density, ρ is the water density, d_{50} is the median particle diameter, α denotes the angle formed between the flow direction and the slope direction, β is the slope angle, φ is the sediment angle of repose, and D_* is a particle size parameter.

Recent studies have extended the conventional Shields parameter to account explicitly for seepage forces generated by pore-pressure gradients within a permeable seabed. Rather than treating seepage as a separate sediment-mobility parameter, these formulations modify the Shields parameter itself through a correction coefficient derived from the force balance acting on a sediment particle. Early formulations considered only the vertical pore-pressure gradient and associated seepage force [27], while subsequent studies extended the approach to two-dimensional seepage, incorporating both horizontal and vertical pore-pressure gradients together with local bed-slope effects [28,29], and later to three-dimensional seepage fields around pile foundations [30]. In the two-dimensional formulation adopted by Zhai and Jeng [29], the modified Shields parameter is expressed as $\theta_{mod} = R\theta$, where R accounts for the seepage force generated by the pore-pressure gradients and the local bed slope. The resulting modified Shields parameter, rather than the conventional Shields parameter, is then used in the bed-load transport formulation, thereby coupling wave-induced seabed response directly to sediment transport and scour development. More recently, Hu and Li [31] incorporated three-dimensional seepage and bed-slope effects into the modelling of sediment incipient motion and scour around a circular pile.

For wave-induced (oscillatory) flows, the Keulegan–Carpenter (KC) number, defined as the ratio of the particle distance covered during an oscillatory cycle to the characteristic length (e.g., pile diameter), influences the nature and intensity of vortex shedding. At low KC values, horseshoe-vortex formation is suppressed, whereas increasing KC promotes larger, more persistent vortices [32]. KC is defined as:

$$KC = U_m T / D \tag{5}$$

where U_m is the maximum undisturbed velocity at the bed, T is the wave period, and D is a characteristic length (e.g., pile diameter).

Experimental studies by Sumer and Fredsøe [33] demonstrated that for a vertical pile exposed to waves, the equilibrium scour depth increases with both KC and the diffraction parameter D/L, where L denotes wavelength. This behaviour is attributed to enhanced

steady streaming generated by the presence of the pile at higher values of these parameters. In oscillatory flow with small KC and D/L, sediment tends to move back and forth without significant net transport. By contrast, strong steady streaming at larger KC and D/L produces a residual current that excavates sediment and inhibits redeposition, thereby deepening scour holes. This trend is valid for relatively low KC values (i.e., $KC < O(1)$), while for larger values (i.e., $KC > 6$), scour depth continues to increase with KC. In the latter case, scour is dominated by vortex structures rather than steady streaming, mainly the horseshoe vortex for $KC < 30$ and vortex shedding at higher values. Consistent with this, Ahmad et al. [34] reported a fourfold increase in equilibrium scour depth when KC increased from 6 to 12.

Structural geometry and orientation also influence local scour. Lancaster et al. [35] employed single-phase numerical simulations and showed that bluff structures with sharper corners developed deeper scour than rounded geometries. Also, when corners faced directly into the flow, vortex formation was intensified, leading to deeper local scour, whereas oblique orientations redistributed scour patterns along the structure sides. Their results further showed that longer structures parallel to the flow promoted larger scour, as vortices were more effectively sustained along the structure length. Importantly, the above impacts of structural geometry were found to be more pronounced at higher KC values. Similar sensitivity to structural configuration has been reported for coastal protection structures, where the type of wave-dissipating block can influence breakwater settlement and overall morphological change [36].

Another parameter that is used in the literature to predict scour depth, although less common than θ, is the Froude number (F_d). Similar to θ, F_d describes sediment mobility by assessing the balance between hydrodynamic forcing and resisting sediment weight. The difference between the two is that θ is a normalised measure of shear stress, while F_d is a normalised measure of velocity, as follows [37]:

$$F_d = \frac{V}{\sqrt{g' d_{50}}},\ g' = \frac{(\rho_s - \rho)}{\rho} g \tag{6}$$

where V is undisturbed flow velocity approaching a structure and g' is reduced gravitational acceleration. As inferred from the experimental study of Oliveto and Hager [37], scour depth increases with F_d following a power-law dependence.

3. Modelling Challenges

From a numerical modelling perspective, reliable representation of scour processes presents several challenges. The turbulent flow structures that drive sediment entrainment and local scour, such as horseshoe vortices, wake vortices, and near-bed coherent motions, often occur at scales smaller than the computational resolution and must therefore be represented through turbulence closure models. Sediment transport is also challenging to model because the relation between sediment fluxes depends on hydrodynamic and soil variables, including bed shear stress, flow velocity, turbulence intensity, sediment concentration, bed slope and grain size [34]. Additionally, predicting bed evolution requires robust morphodynamic treatment of erosion, deposition, bed-load and suspended-load transport, as well as avalanching on sloped beds.

A further complication is the temporal disparity between rapidly evolving hydrodynamic processes and the slower bed morphology evolution. This makes fully coupled simulations computationally demanding, particularly for three-dimensional flows and long-duration processes [38]. Consequently, different time steps are often adopted for hydrodynamic and morphological models, an approach commonly referred to as partial

decoupling or quasi-steady coupling [24,34,39,40]. Although this approach can substantially reduce computational cost, the use of different hydrodynamic and morphological time steps can introduce numerical errors when bed changes become significant within a hydrodynamic update interval. In such cases, sediment transport may be evaluated using a flow field that is no longer consistent with the evolving bed, resulting in lagged flow–bed feedback, over- or under-prediction of bed-level change, and spurious oscillatory erosion and deposition, particularly during rapid scour or strongly coupled flow–sediment conditions [41,42]. In addition, temporal inconsistencies between the computation of sediment fluxes and the subsequent bed morphology update can introduce local or cumulative sediment-mass imbalances at the fluid–bed interface if the exchanged fluxes are not treated conservatively. The morphological time step should also satisfy the stability requirements of the bed-evolution equation, since excessively large time steps or dispersive bed-update schemes can generate non-physical high-frequency oscillations in bed elevation [43]. Therefore, the ratio between hydrodynamic and morphological time steps should be selected according to the strength of flow–bed coupling and the rate of morphological change, with more frequent re-coupling or fully coupled approaches becoming preferable when rapid bed evolution invalidates the quasi-steady assumption.

Reliably resolving the fluid–soil interface remains a significant challenge. The bed surface evolves continuously during scour, requiring numerical schemes to track changes in bed elevation while preserving stability and mass conservation [40,44,45]. Moreover, predicting interface stresses is complicated by the presence of the thin viscous sublayer adjacent to the bed that contains steep velocity, concentration, and stress gradients. Explicitly resolving this sublayer would require a very fine mesh and substantial computational resources. Although wall-function approaches have been developed to address this problem for fluid–solid interface cases [46], their extension to fluid–bed systems is still an active research topic [40].

Another significant challenge lies in the simulation of extreme events, where mechanisms such as plug flow or momentary bed failure can dominate sediment transport. Extreme-event scour is particularly relevant under tsunami loading. Jazaeri et al. [47] reviewed tsunami-induced scour around structures and highlighted the need for improved understanding and numerical modelling of unsteady inundation-driven scour processes and their implications for coastal infrastructure resilience. As shown in the work of Cheng et al. [48], strong horizontal pressure gradients associated with steep-wave passage can destabilise the seabed in ways that are not captured by traditional shear-stress-based transport formulations. Capturing such processes requires advanced multiphase models and high spatial and temporal resolution, which in turn demand considerable computational resources.

4. Classification of Numerical Methods

Numerical models developed to investigate scour processes can be classified according to several criteria, including numerical discretisation framework, the mathematical framework used to represent the sediment phase, and the treatment of particle–particle and fluid–particle interactions. These distinctions, which rely on different assumptions, determine both the computational cost and the physical fidelity of the simulations.

Numerical scour studies are most commonly classified according to their discretisation framework, including the finite-volume method, the Discrete Element Method, the finite element method (FEM), and meshless approaches. Among these, FVM dominates CFD-based scour studies due to its ability to resolve complex hydrodynamics and its compatibility with unstructured meshes, making it well-suited for modelling complex geometries [49]. DEM can be coupled with CFD to enable discrete representation of sediment particles. Meshless

particle-based approaches, such as Smoothed Particle Hydrodynamics (SPH) represent both fluid and sediment phases as moving particles, and have been applied in dam-break and sediment-flushing studies [50]. FEM is preferred for evaluating the structural response of foundations under scoured conditions [5,51–53]. However, because FEM cannot simulate the transient scour process itself, it is not considered further in this review. Using an idealised offshore pile as a reference configuration, Figure 2 schematically illustrates the contrasting discretisation of the fluid and soil domains adopted by the different modelling approaches reviewed in this paper.

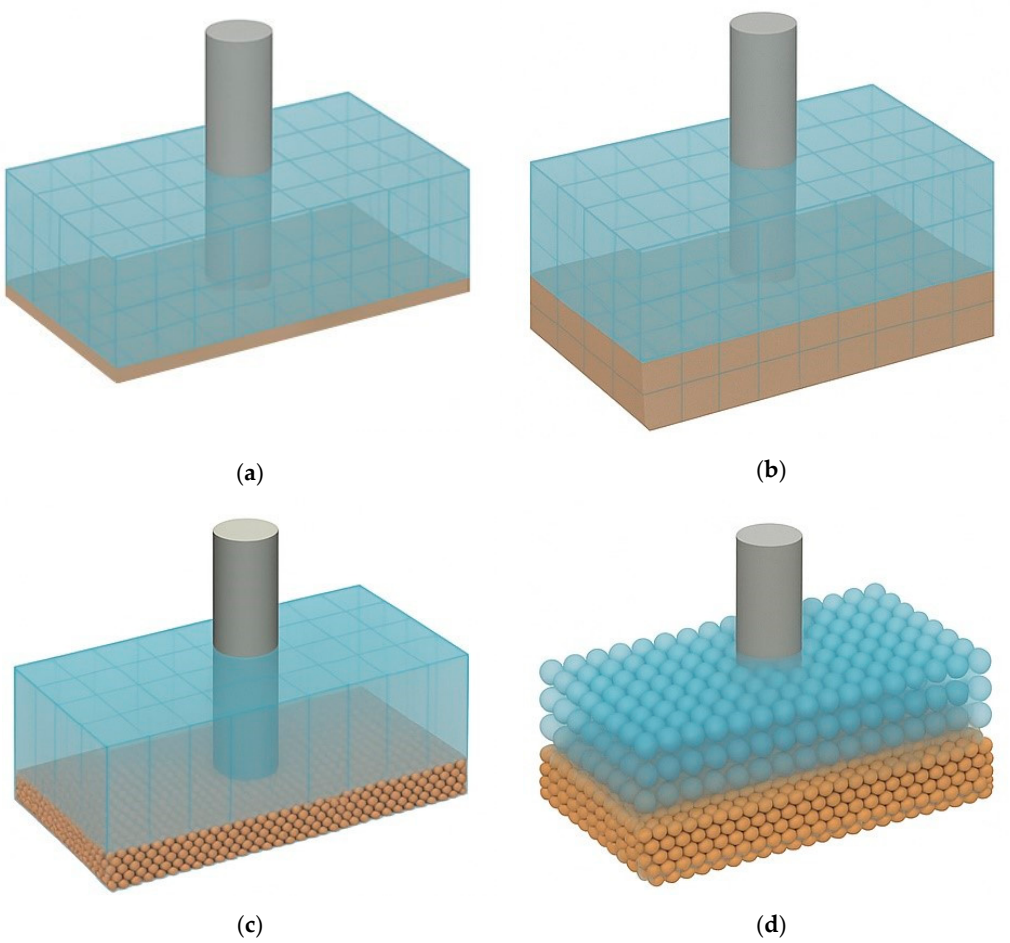


Figure 2. Schematic discretisations of fluid (blue) and soil (brown) domains around an idealised offshore pile for (**a**) single-phase Eulerian, (**b**) two-phase Eulerian, (**c**) CFD–DEM, and (**d**) SPH approaches.

The frameworks used to represent water and sediment flow provide a further basis for classification. Single-phase Eulerian models divide the domain into a water column and a near-bed layer (Figure 2a). Sediment in the water column is treated as a passive scalar with a prescribed settling velocity, while bed-load transport in the lower layer is computed using empirical formulas [49]. Two-phase Eulerian–Eulerian models treat both water and sediment as continuous phases (Figure 2b), with a distinct rheology for the sediment phase. A third approach is the Eulerian–Lagrangian or CFD–DEM method. In this method, the fluid is treated as a continuous phase and solved on a Eulerian grid, while sediment particles are represented as discrete entities (Figure 2c) whose motion is resolved in the Lagrangian framework. The Lagrangian framework may also be applied to the fluid phase through mesh-free methods such as SPH (Figure 2d).

5. Finite-Volume Method (FVM)

The finite-volume method is the most widely used computational framework in scour modelling, particularly in CFD simulations. It discretises the domain into a finite number of control volumes and enforces conservation of mass and momentum within each volume. FVM is well-suited to handling complex geometries and large deformations, and it is highly compatible with sediment-transport modelling. Implemented in open-source and commercial CFD solvers such as OpenFOAM, REEF3D, and FLOW-3D, FVM has been applied to scour problems ranging from monopiles [25,40,45,54], jacket structures [34], and tandem piers [55] to breakwaters [56], aprons [48,49], bluff bodies [35], and pipelines [24,57,58]. In recent years, FVM-based studies, validated against experimental scour data, have made significant contributions to advancing modelling methodologies and enhancing the understanding of scour mechanisms. The following subsections review single-phase and two-phase Eulerian approaches within the FVM framework.

5.1. Single-Phase Models

5.1.1. Hydrodynamic and Sediment Transport Coupling

In classical single-phase scour modelling, the numerical framework generally couples two main components: a hydrodynamic solver and a sediment-transport model. The hydrodynamic CFD solver resolves the flow field, turbulence quantities, and near-bed shear stresses induced by waves and currents. It then provides this information to the sediment-transport model, which computes the associated sediment fluxes and updates the seabed morphology through the Exner equation. The updated bed geometry and sediment concentration are then transferred to the subsequent hydrodynamic solution. This exchange of information over successive time steps is summarised schematically in Figure 3.

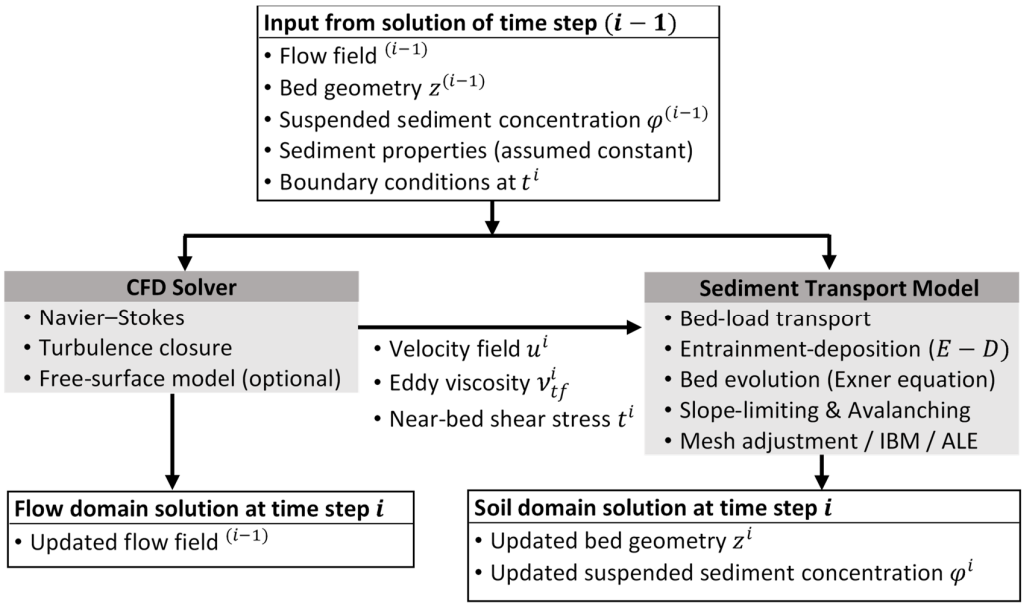


Figure 3. Coupling between CFD solver and sediment-transport model.

The computational domain is divided into two sublayers (upper and lower) that are dynamically linked. The upper layer simulates the water column, where the hydrodynamic solver usually resolves the flow using Reynolds-Averaged Navier–Stokes (RANS) approach or the more computationally expensive Large Eddy Simulation (LES) approach. The incompressible RANS equations are solved either in a depth-integrated form, by solving vertically averaged RANS equations, or in a depth-resolving form, by resolving vertical profiles of flow and turbulence [49]. Turbulence is typically parameterised using closures such as the

k-ε [59], k-ω [60] and LES [61] class of models. Suspended sediment within this layer is assumed to be dilute, meaning its volume fraction is sufficiently small for particle–particle interactions and its influence on the flow's density, viscosity, turbulence, or momentum is negligible. That is, the presence of sediment does not exert any influence on the hydrodynamic solution. Instead, it is modelled as a passive scalar that is advected and diffused by the resolved flow, with an additional constant downward component representing the sediment's settling velocity under gravity. This approach enables suspended-sediment transport to be modelled as a function of the resolved hydrodynamics, while maintaining the computational efficiency of a single-phase approach.

The lower layer corresponds to the near-bed bed-load zone, where sediment is moved primarily by rolling, sliding, and saltation along the bed. At this layer, the sediment-transport rate is estimated using empirical formulations that rely on bed shear stress relationships, which incorporate the resolved hydrodynamic forces and sediment grain size. Such three widely adopted formulations are those proposed by Meyer-Peter and Müller [62], van Rijn [63], and Engelund and Fredsoe [64]. Building on this formulation, Dixen et al. [65] introduced a modification to account for additional bed-load transport induced by turbulence associated with fluid–structure interaction, such as the horseshoe vortex and lee-wake flow. Turbulence intensity, predicted by a k-ω SST closure in the CFD model, was used as input to these empirically calibrated relations, which were coupled with the Engelund and Fredsøe framework. This extension was shown to produce substantially larger predicted scour depths and faster scour development, in closer agreement with laboratory observations. The sediment-transport formulations are coupled with the sediment continuity equation (Exner equation) to predict the morphological evolution of the bed.

Within single-phase local-scour modelling, sediment transport may be represented using bed-load transport alone or through a combination of bed-load and suspended-load formulations. Bed-load-only models are generally adopted when sediment motion remains concentrated close to the bed, while suspended-load transport is additionally represented when particles are substantially entrained into the water column. Both approaches have been applied in local-scour simulations, with examples of bed-load-only formulations provided by Roulund et al. [11] and Dixen et al. [65], and combined bed-load and suspended-load formulations by Baykal et al. [66] and Ahmad et al. [34,39].

5.1.2. Free-Surface Modelling

Free-surface modelling is generally unnecessary in scour simulations at very low Froude numbers ($F_d < 0.2$), which correspond to near-current conditions. However, for larger Froude numbers and particularly in wave-induced scour problems, free-surface effects become non-negligible and must be modelled explicitly within numerical simulations [39].

The VOF method is a well-established and validated approach for tracking free-surface flows and has been widely employed in coastal hydrodynamic applications [67]. In single-phase scour simulations, free-surface effects are typically resolved using the level-set method [34,35], which represents the free surface through a function $\varphi\left(\vec{x}, t\right)$, originally proposed by Osher and Sethian [68] and later further developed by Peng et al. [69]. This function evolves over time (t) and depends on both the signed spatial coordinate ($\vec{x}$) and the velocity field ($\vec{u}$). The sign of φ indicates the phase; specifically, it is negative in phase 1, positive in phase 2, and zero at the interface, while $\vec{u}$ is obtained from the RANS equations. After defining the initial condition $\varphi\left(\vec{x}, 0\right)$, the function's evolution over time

is determined by solving the partial differential Equation (7), known as the convection equation. Once φ is computed, the interface is located at positions where $\varphi = 0$.

$$\frac{\partial \varphi}{\partial t} + \vec{u} \cdot \nabla \varphi = 0 \tag{7}$$

However, the level-set method has limited applicability in cases with strong air–water interactions, such as breaking waves or air entrapment, where explicit modelling of the air phase becomes necessary. In such scenarios, two-phase approaches such as the Volume-of-Fluid (VOF) or Coupled Level Set–VOF (CLSVOF) methods are more appropriate, as they resolve both water and air phases and better capture complex free-surface dynamics [70].

5.1.3. Morphological Models

In the single-phase framework, the bed morphology is commonly updated using the Exner sediment continuity equation, that ensures sediment-mass conservation and, thus, links the divergence of total sediment transport to local erosion and deposition. The morphological and hydrodynamic models can be fully or partially coupled, the latter employing larger morphological time steps than the hydrodynamic solution to reduce computational cost [24,34,39,40]. The Exner equation, describing the temporal evolution of the bed elevation based on the principle of mass conservation, is expressed as:

$$\frac{\partial z}{\partial t} + \nabla \cdot q_b(\tau(u)) = 0 \tag{8}$$

where t is time, z is seabed level, and q_b is the rate of bed transport, which is a function of bed shear stress τ and flow velocity u. For a 3D model in which suspended load is included, the above equation expands as [39]:

$$\frac{\partial z}{\partial t} + \frac{1}{1-n} \cdot \left[\frac{\partial q_{b,x}}{\partial x} + \frac{\partial q_{b,y}}{\partial y} \right] + E - D = 0 \tag{9}$$

where $q_{b,x}$ and $q_{b,y}$ represent the bed-load transport rate in the x and y directions, respectively, n is sediment porosity, E is the entrainment rate from bed-load and D is the deposition rate. The quantity $(E - D)$ corresponds to the balance of entrainment and deposition at the bed-load–suspension interface and can be determined using Equation (10) proposed by Wu et al. [71].

$$E - D = \omega_s \cdot (c_{b*} - c_b) \tag{10}$$

where ω_s is the sediment settling velocity, c_b is the sediment concentration at the interface, and c_{b*} is the equilibrium concentration. In the finite-volume method, this interface, the top of the bed-load layer, is located at a distance δ_b above the seabed. The thickness of the bed-load layer δ_b is commonly taken as two times the median sediment grain ($2d_{50}$) for flat beds and as 2/3 of the roughness height for beds with a sinusoidal surface [71]. Since δ_b lies below the lowest grid point (lgp) above the bed, where concentration c_{lgp} is known, interpolation is required to obtain c_b at δ_b. Following Wu et al. [71], the concentration distribution can be assumed to follow an equilibrium distribution, leading to the formulation given in Equation (11). The sediment settling velocity, ω_s, can be obtained from Equation (12) proposed by Soulsby [22] for natural sands with irregular grains of any D_*.

$$c_b = c_{lgp} + c_{b*} \cdot \left[1 - e^{(\omega_s \sigma_c / \nu_{tf})(z_{lgp} - \delta_b)} \right] \tag{11}$$

$$\omega_s = \frac{v}{d_{50}} \cdot \left[\left(10.36^2 + 1.049 D_*^3 \right)^{0.5} - 10.36 \right] \tag{12}$$

where σ_c is the Schmidt number, ν_{tf} is the eddy viscosity, and D_* is a particle size parameter defined in Equation (4). The equilibrium concentration c_{b*}, according to van Rijn [72], is defined as:

$$c_{b*} = 0.015 \cdot \frac{d_{50} T^{1.5}}{\delta_b D_*^{0.3}} \quad (13)$$

where T is a non-dimensional parameter characterising bed shear stress, the definition of which can be found in [71].

To account for slope instability, slope effects and sand-slide (avalanching) algorithms are often incorporated, ensuring that the bed slope remains below the angle of repose (φ). This angle depends on the orientation between the bed slope and velocity vector—being larger for downslope than upslope conditions [9,39]—and on soil properties such as cohesion, grain size, and shape [73]. Burkow and Griebel [73] proposed a model for single-phase numerical analyses that limit bed slopes below tan φ. Their approach recalculates slopes at each time step and, if limits are exceeded, iteratively redistributes soil mass to adjacent cells until all slopes satisfy the criterion. Additionally, the slope within the scour hole influences the evolution of erosion; therefore, the critical shear stress in sediment-transport formulations should explicitly account for slope effects, as discussed earlier and indicated in Equation (3) [35].

Although mesh deformation is typically applied only in the vertical (z) direction—an assumption valid for vertical piles under axisymmetric conditions—inclined-piles induce additional horizontal deformations. As noted by Liu et al. [44], displacement corrections must be incorporated into sand-slide models to ensure that the evolving bed surface conforms to the sloping contour of the pile. Without such corrections, the mesh boundary may intersect or detach from the inclined pile surface, resulting in unrealistic scour patterns and numerical inconsistencies. To address this, Liu et al. [44] proposed introducing horizontal displacement components for an inclined pile whose axis (generatrix) is described by the direction cosines ($cos\alpha$, $cos\beta$, $cos\gamma$):

$$\Delta x_b = \omega_i \Delta z_b \cdot cos\alpha / cos\gamma, \Delta y_b = \omega_i \Delta z_b \cdot cos\beta / cos\gamma \quad (14)$$

where ω_i is a weighting factor defined as $\cos\left(\frac{2\pi}{D} \cdot d\right)$, with D denoting the pile diameter and d the distance from the pile-bed intersection. The direction cosines define the orientation of the inclined pile relative to the global Cartesian coordinate system and are used to derive the horizontal x- and y-displacement components from the computed vertical bed-elevation change. In this way, the resulting three-dimensional bed-mesh displacement is coordinated with the inclined-pile geometry and can be introduced into the sand-slide model so that the bed-mesh deformation conforms to the inclined pile contour. This coordinate-based decomposition ensures that mesh nodes adjacent to the pile are displaced consistently with the pile inclination, rather than purely along the global vertical direction. Liu et al. [44] further emphasised that coordination between the motion of the bed mesh and that of the inclined-pile mesh is important for numerical convergence, since excessive distortion of the pile-adjacent mesh may otherwise develop during morphological evolution. The weighting function ω_i is introduced to constrain the horizontal displacements and mitigate excessive mesh skewness of near-bed mesh cells that could otherwise lead to numerical instability.

5.1.4. Modelling Evolving Beds

Bed morphology evolves dynamically, which in principle would require continuous remeshing to match the moving boundary. In one class of methods, often referred to as adaptive meshing, bed-level changes are first computed at the cell centre (Δh_b) from the Exner equation. These changes are then interpolated to the mesh vertices ($\Delta h_{b,node}$) along the bed boundary by following an area-weighted method proposed by Liang et al. [24].

The weight is computed for each (j) of the m elements surrounding a node considering the elements area S_j as per Equation (15), while $\Delta h_{b,node}$ is computed as per Equation (16).

$$\lambda_j = \frac{S_j}{\sum_{j=1}^{m} S_j} \tag{15}$$

$$\Delta h_{b,node} = \sum_{j=1}^{m} \lambda_j \Delta h_{b,j} \tag{16}$$

Once nodal displacements at the bed nodes are computed, the resulting deformations are propagated into the interior mesh. Liang et al. [24] combined spring smoothing with local remeshing to maintain mesh quality. Spring smoothing distributes the boundary displacement through neighbouring nodes, while local remeshing regenerates cells that become excessively distorted. This combination allows the mesh to conform to the evolving bed while reducing the risk of cell overlap and numerical instability. Alternatively, bed displacements can be propagated through the computational domain by solving a Laplace equation for mesh motion [74,75]. On this basis, the Arbitrary Lagrangian–Eulerian (ALE) method can also be employed [44,76]. ALE allows the computational mesh to deform with the evolving bed while prescribing mesh motion independently of material motion. Nodes close to the bed follow the boundary deformation, whereas the interior mesh remains comparatively fixed to preserve mesh quality. The resulting mesh displacement field can be obtained by solving a Laplace equation:

$$\nabla \cdot (\gamma \nabla \boldsymbol{d}) = 0 \tag{17}$$

where $\boldsymbol{d}$ is mesh displacement vector and γ is a diffusion coefficient. The updated bed elevation defines the boundary conditions of the equation, whose solution distributes the deformation smoothly throughout the computational domain and prevents excessive distortion.

Updating the mesh at every time step is computationally expensive; therefore, single-phase scour simulations often employ the immersed boundary method (IBM). IBM is a numerical technique for handling complex or moving geometries in CFD without requiring a body-fitted mesh, which has been used in both fluid–structure interaction problems [46] and scour problems [34,39]. In IBM, the computational grid remains fixed while the evolving seabed is represented as an immersed boundary, with its influence on the flow imposed through nearby cells, typically using a local ghost-cell approach.

In this approach, cells located below the immersed boundary are designated as ghost cells, while the rest are treated as fluid cells. Following the local directional ghost-cell method [77], for each ghost cell, an image point is defined by projecting the ghost-cell centre along the boundary-normal direction into the fluid region. Flow variables at the image point are obtained by interpolation from neighbouring fluid cells, and ghost-cell values are assigned to enforce the prescribed velocity, pressure, and sediment boundary conditions. The directional projection applies these conditions at the actual boundary location and is therefore better suited to curved or inclined geometries than grid-aligned interpolation approaches [78–80].

A further challenge in single-phase scour modelling is the reliable representation of near-bed shear stresses. Conventional CFD wall functions avoid explicit resolution of the viscous sublayer by relating velocity at the first off-wall grid point to wall shear stress through semi-empirical relationships. However, their direct application to a mobile seabed is limited because bed geometry, roughness, and slope evolve during scour, while the resulting shear stresses must also be coupled to the sediment-transport model through

the Shields parameter (Equations (1)–(3)) and hence the initiation of motion. Rigid-wall functions therefore fall short in this context, as they lack (i) dynamic updating to account for evolving bed geometry, (ii) slope effects, and (iii) explicit coupling with morphodynamics.

To address this limitation, Song et al. [40] proposed a wall-function formulation embedded in IBM to compute bed shear stresses consistently on evolving sand beds. In this approach, the shear velocity at the bed (u_τ) is related to flow velocity u in the fluid field at a distance y from the bed through the log-law relationship:

$$u^+ = \frac{1}{\kappa}\ln\left(E' y^+\right) \tag{18a}$$

$$u^+ = \frac{u}{u_\tau} \tag{18b}$$

$$y^+ = \frac{u_\tau y}{\nu} \tag{18c}$$

where u^+ and y^+ are a measure of dimensionless velocity and wall distance, respectively, E' accounts for bed roughness, κ is a von Kármán constant and ν is kinematic viscosity.

Equation (18a) is solved iteratively (Newton–Raphson) at the image point to obtain the local shear velocity u_τ and corresponding bed shear stress $\tau = \rho {u_\tau}^2$. These stresses evolve with the changing bed topography and are directly coupled to the sediment-transport and Exner formulations. Current implementations nevertheless neglect explicit slope and bed-permeability effects, and the IBM wall-function approach remains computationally more expensive than ALE methods, particularly at high Reynolds numbers [40].

5.1.5. Advantages and Limitations

Single-phase sediment-transport models have relatively low computational demand compared with two-phase CFD approaches and can generally employ coarser spatial grids and larger time steps [49]. They can reproduce key scour trends, including sensitivity to hydrodynamic parameters such as the KC number, and incorporate realistic boundary conditions, slope effects, and avalanching. They have proven useful for predicting long-term morphological changes in littoral environments, particularly when flow velocities are modest and suspended sediment has little feedback on the hydrodynamics [18,49].

Under high-velocity or strongly turbulent conditions, dense near-bed sheet-flow layers may develop. These conditions cannot be represented reliably by single-phase models because sediment feedback on the carrier flow is neglected. Suspended load may be neglected under near-clear-water conditions where bed-load transport dominates [18,24,65], but its omission outside this regime can significantly affect predicted scour and deposition. Baykal et al. [66], for example, reported an underestimation of upstream scour by nearly 50%, while Liang et al. [24] found overestimation of downstream deposition when suspended transport in the wake was neglected. Single-phase models also neglect particle–particle interactions, dense particle–flow interactions, and delayed entrainment of particles into turbulence. Furthermore, the reliability of commonly used transport formulas under highly unsteady conditions remains uncertain [49]. Coarse spatial resolution and reliance on RANS turbulence closures may also under-resolve critical three-dimensional vortex structures such as horseshoe and lee-wake vortices [81], which contribute strongly to local-scour development.

A further limitation is the dependence on empirical sediment-transport formulations. Because the bed is treated as a morphodynamic boundary rather than an interacting granular phase, sediment mobility must be prescribed through semi-empirical transport relations. Lancaster et al. [35] showed that replacing the calibrated van Rijn [63] formulation with Meyer-Peter and Müller [62] or Engelund and Fredsøe [64] produced overpredictions

of 65% and 77%, respectively, at the downstream corner of the structure. This sensitivity highlights the need for careful selection and calibration of the transport formulation.

5.1.6. Engineering Applicability

Single-phase Eulerian morphodynamic models are particularly suitable for preliminary and large-scale scour assessments, clear-water or weakly live-bed conditions, and parametric engineering studies where computational efficiency is important. They are less suitable in cases involving dense sheet flow, strong sediment feedback, momentary bed failure, and problems where particle-scale mechanisms control the response. The main engineering limitation of single-phase CFD-based scour simulations is their sensitivity to the selected empirical sediment-transport formulation and associated calibration dataset.

5.2. Two-Phase Eulerian–Eulerian Models

5.2.1. Governing Equations and Conceptual Framework

The Eulerian–Eulerian two-phase modelling framework has emerged as one of the most advanced methodologies for simulating sediment transport and scour processes in complex hydraulic environments. Unlike single-phase models, which rely heavily on empirical transport formulas and the division of sediment fluxes into suspended and bed-load components, the Eulerian–Eulerian approach treats both the carrier fluid and the sediment phase as interpenetrating continua. Both phases coexist in the same space but are described by their own field variables. Each phase satisfies its own mass and momentum conservation equations, while the two phases interact through interphase momentum-transfer terms. Particle–particle interactions are not rigorously resolved in such models, but they are considered through stress closure models for the sediment phase [45,48,82].

Because it is impractical to resolve the detailed motion of every individual sediment grain and the surrounding fluid, the governing equations for two-phase flow are derived by applying averaging procedures to the Navier–Stokes equations [48]. This averaging is performed over a length scale that exceeds the particle diameter, to filter out particle-level fluctuations, but is still smaller than the characteristic macroscopic flow scale, so that flow heterogeneities at engineering scales are preserved. Two averaging approaches are commonly used: ensemble averaging [83], which computes a statistical mean across many possible system realisations, and *volume averaging* [84], which computes local averages over representative spatial volumes containing both phases. The outcome of the averaging procedure is a set of coupled partial differential equations that describe the evolution of the fluid and sediment phases. For each phase, mass conservation is expressed through a continuity equation for the phase volume fraction and velocity field, while momentum conservation yields a balance between inertial, pressure, viscous, and gravitational forces, supplemented by interphase momentum-exchange terms such as drag, lift, buoyancy or added-mass forces [49]. As provided by Cheng et al. [48], the mass conservation equations are defined by Equations (19) and (20), while the momentum equations are defined in Equations (21) and (22) for the fluid and sediment phases, respectively.

$$\frac{\partial(1-\varphi)}{\partial t} + \nabla\left((1-\varphi)\boldsymbol{u_f}\right) = 0 \tag{19}$$

$$\frac{\partial \varphi}{\partial t} + \nabla(\varphi \boldsymbol{u_s}) = 0 \tag{20}$$

$$\rho_f(1-\varphi)\left(\frac{\partial \boldsymbol{u_f}}{\partial t} + \boldsymbol{u_f}\cdot\nabla\boldsymbol{u_f}\right) = -(1-\varphi)\nabla p_f + \nabla\boldsymbol{\tau_f} + \rho_f(1-\varphi)\boldsymbol{g} + (1-\varphi)\boldsymbol{f} + \boldsymbol{M_{fs}} \tag{21}$$

$$\rho_s\varphi\left(\frac{\partial \boldsymbol{u_s}}{\partial t} + \boldsymbol{u_s}\cdot\nabla\boldsymbol{u_s}\right) = -\varphi\nabla p_f - \nabla p_s + \nabla\boldsymbol{\tau_s} + \rho_s\varphi\boldsymbol{g} + \varphi f - \boldsymbol{M_{fs}} \tag{22}$$

where φ is the sediment concentration per volume, $(1-\varphi)$ is the fluid concentration, $\boldsymbol{u_f}$ and $\boldsymbol{u_s}$ are the fluid and sediment velocity fields, ρ_f and ρ_s are densities and p_f and p_s are pressures for the two phases. The gravity field is represented by $\boldsymbol{g} = [0\,0\,-9.81]$, and $\boldsymbol{f}$ represents pressure gradient that externally drives the flow, while $\boldsymbol{M_{fs}}$ denotes the momentum transfer between the phases. $\boldsymbol{\tau_f}$ is the fluid stress accounting for both viscous and turbulent Reynolds stresses, while $\boldsymbol{\tau_s}$ is the sediment shear stress. This separation is particularly relevant for hollow foundations, such as open-ended pipe piles. In such cases, the sediment enclosed by the foundation may constitute an internal soil plug whose gravitational contribution needs to be distinguished from the hydrodynamic forcing acting on the sediment [85]. In the Eulerian–Eulerian formulation considered here, this distinction is inherently preserved. In Equation (22), the self-weight of the internal sediment is represented independently by the body-force term $\rho_s \varphi g$, while hydrodynamic forcing is represented separately through the fluid-pressure gradient, external flow forcing and interphase momentum-transfer terms. Therefore, when the governing equations are applied to internal scour, the gravitational contribution associated with the remaining internal sediment should be retained independently rather than incorporated into the external hydrodynamic forcing.

The two phases are coupled because the pressure field is common to both phases and the interphase forces enter the respective momentum equations with equal magnitude and opposite sign. These equations therefore govern the spatiotemporal evolution of the sediment concentration, as well as velocity and stress fields of both fluid and sediment, but they contain additional terms representing particle stresses and turbulence–sediment interactions that must be closed empirically. Specifically, for the computation of sediment pressure and shear stress, p_s and $\boldsymbol{\tau_s}$, a particle stress closure is required. The sediment phase is modelled as a continuum with its own rheological properties because of the dual fluid–solid behaviour it exhibits depending on sediment concentration, as further detailed in Section 5.2.2. Similarly, an interphase momentum-transfer closure is needed for the computation of $\boldsymbol{M_{fs}}$ [48], as described in Section 5.2.3.

5.2.2. Granular-Stress Closure

Unlike simple fluids, sediment beds exhibit both solid-like and fluid-like characteristics depending on local shear, packing, and stress conditions [49,86,87]. They flow under shear like a viscous fluid when dilute, yet sustain finite shear stresses without deformation when densely packed. When the bed is mobilised, dense granular regions coexist with dilute suspensions, leading to strong spatial variations in the effective stress response of the sediment phase. A rheological closure is therefore essential in Eulerian–Eulerian two-phase models to relate the sediment-phase stress tensor, $\boldsymbol{\tau_s}$, and pressure, p_s, to measurable flow variables such as the sediment concentration φ and strain rate $\dot{\gamma}$ [48,49].

In granular-flow modelling, distinct rheological closures apply to specific concentration ranges: kinetic theory of granular flow for dilute to moderately dense suspensions ($\varphi \lesssim 0.3$), hybrid or $\mu(I)$-type models for dense regimes ($0.3 \lesssim \varphi \lesssim 0.6$), and frictional or viscoplastic closures as φ approaches maximum packing ($\varphi \gtrsim 0.6$). Traditional single-phase or empirical transport formulations assume Newtonian behaviour with constant viscosity, but this approximation fails within dense near-bed layers where particle contacts dominate and stresses become nonlinear [49,88]. In these regions, the sediment phase exhibits non-Newtonian, rate-dependent rheology. Two-phase approaches therefore employ constitutive laws derived from granular-flow theory to represent both collisional and frictional regimes [48,49,89,90]. The constitutive behaviour of the sediment phase governs the transfer of shear and normal stresses within the granular medium and controls the transition from static to mobile conditions. Various rheological closures have been proposed

to represent the effective stress–strain relationship of the sediment phase across different concentration regimes.

In the dilute to moderately dense regime ($0.08 < \varphi < 0.3$), particle collisions dominate momentum exchange, and the kinetic theory of granular flow (KTGF) provides an appropriate rheological framework [45]. KTGF treats the sediment phase analogously to gas and introduces a granular temperature, Θ, defined as one-third of the velocity fluctuations. The constitutive relations for sediment collisional pressure and shear stress, p_{sc} and $\boldsymbol{\tau_{sc}}$, can be expressed as follows. Equation (23) follows Ding and Gidaspow [91], Equation (24) adopts the radial distribution function proposed by Torquato [92], and Equation (25) follows Gidaspow [93], as implemented by Cheng et al. [48]:

$$p_{sc} = \rho_s \varphi [1 + 2(1+e)\varphi g_{s0}]\Theta, \tag{23}$$

$$g_{s0} = \begin{cases} \frac{2-\varphi}{2(1-\varphi)^3}, \varphi < \varphi_t \\ \frac{2-\varphi_t}{2(1-\varphi_t)^3} \cdot \frac{\varphi_p - \varphi_t}{\varphi_p - \varphi}, \varphi_t < \varphi < \varphi_p \end{cases}, \tag{24}$$

$$\boldsymbol{\tau_{sc}} = 2\mu_{sc}\boldsymbol{D_s} + \left(\lambda_{sc} - \frac{2}{3}\mu_{sc}\right)(\nabla \boldsymbol{u_s})\delta_{ij}, \tag{25}$$

$$\boldsymbol{D_{s,ij}} = \frac{1}{2}\left(\frac{\partial u_{s,i}}{\partial u_{s,j}} + \frac{\partial u_{s,j}}{\partial u_{s,i}}\right) \tag{26}$$

where e is the coefficient of restitution, $\boldsymbol{D_s}$ is a strain-rate tensor for the velocity field, δ_{ij} is the Kronecker delta, μ_{sc} is the collisional particle shear viscosity and λ_{sc} is the bulk viscosity. The parameter g_{s0} accounts for the increasing collision frequency as the sediment concentration approaches maximum packing. The expression adopted in Equation (24), originally proposed by Torquato [92] for hard spheres and later applied to two-phase sheet-flow modelling by Hsu et al. [94], depends on the maximum packing fraction φ_p and a threshold packing fraction φ_t associated with the transition towards more ordered particle arrangements. For 2D problems, $\varphi_p = 0.82$ and $\varphi_t = 0.69$, while for 3D cases $\varphi_p = 0.64$ and $\varphi_t = 0.49$.

Various viscosity definitions can be found in the literature [90,91,93,95]; for brevity, only those incorporated by Cheng et al. [48] in the OpenFOAM CFD tool and which later have found wide application [45,49,81,82] are presented:

$$\mu_{sc} = \rho_s d\sqrt{\Theta}\left[\frac{4\varphi^2 g_{s0}(1+e)}{5\sqrt{\pi}} + \frac{\sqrt{\pi} g_{s0}(1+e)(3e-1)\varphi^2}{15(3-e)} + \frac{\sqrt{\pi}\varphi}{6(3-e)}\right] \tag{27}$$

$$\lambda_{sc} = \frac{4}{3}\rho_s d\varphi^2 g_{s0}(1+e)\sqrt{\frac{\Theta}{\pi}} \tag{28}$$

KTGF reliably represents collisional stresses in suspension layers but tends to overpredict mobility in dense near-bed regions where enduring contacts prevail [49]. When the packing fraction increases ($0.3 < \varphi < 0.6$), sediment deformation is slow, collisions are no longer instantaneous and the stress transmission becomes frictional [90]. Hybrid frictional–collisional models therefore combine KTGF with a frictional closure above a threshold sediment concentration. A widely adopted formulation is that of Johnson and Jackson [90], in which the total granular stress is expressed as the sum of collisional $\boldsymbol{\tau_{sc}}$ and frictional $\boldsymbol{\tau_{sf}}$ components (Equation (29)). The frictional component may be expressed in terms of the normal frictional stress p_{sf} and internal friction angle φ_f, following the Coulomb criterion

(Equation (30)). The frictional stress p_{sf} can be defined as per Equation (31) and adds up to the collisional stress p_{sc} to compute the total particle stress p_s (Equation (32)).

$$\boldsymbol{\tau_s} = \boldsymbol{\tau_{sc}} + \boldsymbol{\tau_{sf}} \tag{29}$$

$$\boldsymbol{\tau_{sf}} = p_{sf} sin\varphi_f \tag{30}$$

$$p_{sf} = \begin{cases} 0, & \varphi < \varphi_t \\ F\frac{(\varphi-\varphi_t)^m}{(\varphi_p-\varphi)^n}, & \varphi > \varphi_p \end{cases} \tag{31}$$

$$p_s = p_{sc} + p_{sf} \tag{32}$$

The frictional-pressure formulation in Equation (31) provides a smooth transition from collisional to enduring-contact behaviour and increases rapidly as the sediment concentration approaches maximum packing. Its empirical coefficients F, m and n control the magnitude and rate of this increase and therefore require calibration against representative experimental or DEM data [48,49]. Appropriate calibration is necessary to reproduce an immobile bed beneath a mobile sediment layer [48].

An alternative is provided by the $\mu(I)$ rheology, also called the dense granular-flow rheology. This was first introduced by Jop et al. [96] to capture the flow behaviour of dense, dry granular materials through a viscoplastic continuum model. Unlike kinetic theory, which assumes instantaneous binary collisions, the $\mu(I)$ formulation accounts for enduring contacts and frictional stress transmission between particles. In this approach, the granular material is prescribed as an incompressible viscoplastic fluid, with the shear-to-normal stress ratio governed by the inertial number (I), a dimensionless measure of the relative importance of shear deformation to confining pressure:

$$I = \frac{\dot{\gamma} d}{\sqrt{P/\rho_s}} \tag{33}$$

where $\dot{\gamma}$ is the shear rate, P the normal stress (isotropic pressure in 3D conditions), d the particle diameter, and ρ_s the particle density. The constitutive relationship connecting the shear stress τ_s and the normal stress P is then given as:

$$\tau_s = \mu(I) P \tag{34}$$

where $\mu(I)$ denotes the effective friction coefficient, which evolves with I as:

$$\mu(I) = \mu_s + \frac{\mu_2 - \mu_s}{\frac{I_0}{I} + 1} \tag{35}$$

where μ_s and μ_2 represent the minimum (yield) and maximum (high-shear) friction coefficients, respectively, and I_0 controls the transition between quasi-static and inertial regimes. These parameters are material-dependent and should be determined from rheological data representative of the granular material considered. In the calibration procedure described by Jop et al. [97], μ_s and μ_2 were obtained from an experimentally calibrated basal-friction law for steady inclined-plane flows, while I_0 was derived analytically using parameters determined from those experiments.

The three-dimensional generalisation proposed by Jop et al. [96] defines the internal stress tensor $\boldsymbol{\sigma}$ and shear stress $\boldsymbol{\tau_s}$ as:

$$\boldsymbol{\sigma} = \sigma_{ij} = -P\delta_{ij} + \boldsymbol{\tau_s} \tag{36}$$

$$\boldsymbol{\tau_s} = \tau_{ij} = \eta \dot{\gamma}_{ij} \tag{37}$$

where the effective viscosity η and strain-rate tensor $\dot{\gamma}_{ij}$ are defined as:

$$\eta = \frac{\mu(\mathrm{I})\mathrm{P}}{|\dot{\gamma}|} \tag{38}$$

$$\dot{\gamma}_{ij} = \frac{\partial u_i}{\partial u_j} + \frac{\partial u_j}{\partial u_i}, |\dot{\gamma}| = \sqrt{\frac{1}{2}\dot{\gamma}_{ij}\dot{\gamma}_{ij}} \tag{39}$$

As the shear rate vanishes ($|\dot{\gamma}| \to 0$), the inertial number $I \to 0$, implying $\mu(I) \to \mu_s$ and $\eta \to \infty$. This divergence of effective viscosity implies that particles resist deformation as a rigid solid and ensures the existence of a yield criterion, derived from Equations (34) and (35):

$$\tau_s > \mu_s P \tag{40}$$

Below the limit $\mu_s P$, the granular material behaves as a rigid solid, while above the limit, it yields and flows as a viscoplastic fluid.

Forterre and Pouliquen [98] expanded the $\mu(I)$ rheology to a broader range of dense granular flows by allowing both the effective friction coefficient and particle volume fraction to vary with the inertial number. This refinement accounts for weak compressibility effects and improves the model's applicability to more complex, non-homogeneous flow conditions. More recent extensions of the $\mu(I)$ rheology incorporate nonlocal effects through granular-fluidity formulations [99–101]. These formulations improve predictions of creeping flows and spatially heterogeneous shear zones and are therefore promising for modelling sediment mobilisation and scour onset in densely packed beds.

The classical $\mu(I)$ formulation is principally applicable to cohesionless materials in the grain-inertia regime. For sufficiently fine submerged sediments, viscous effects may instead dominate grain inertia. Boyer et al. [102] therefore formulated an analogous friction law in terms of the viscous number, with the rheological coefficients determined from pressure-controlled suspension experiments. Chauchat et al. [49] subsequently incorporated such regime-dependent rheologies into the two-phase sediment-transport framework implemented in SedFOAM. For cohesive sediments, the effective friction has been shown to depart more slowly from its quasi-static limit than for cohesionless grains [103], which may lead to a different fitted I_0. However, cohesion also introduces an additional stress scale that is not represented in the classical formulation, and its effects therefore cannot generally be represented by recalibration of I_0 alone. Studies of cohesive granular flows have therefore extended the rheology by introducing an additional cohesion-dependent parameter or stress contribution [103,104]. More recently, Blatny et al. [105] incorporated cohesion through a modified effective pressure used in the definition of the inertial number, rather than simply adjusting I_0. Consequently, application to cohesive marine sediments or silts requires material-specific rheological characterisation and explicit representation of cohesion.

At high Reynolds numbers, where turbulent fluctuations drive intergranular motion, a turbulent extension of the $\mu(I)$ rheology has been proposed by introducing a turbulent inertial number based on shear velocity [106]. These developments provide a continuous rheological framework spanning laminar, collisional, and turbulent granular regimes, enabling modern two-phase models such as *SedFOAM* [49] to reproduce the transition from static bed to sheet flow and suspension.

5.2.3. Closure Models for Interphase Interactions

Closure models for interphase interactions are essential for describing the exchange of momentum, $\boldsymbol{M_{fs}}$ appearing in Equations (21) and (22), between the fluid and sediment phases. Drew [83] decomposed the interphase momentum term into distinct contributions associated with the interphase velocity, interphase pressure, and interphase force density. These are typically interpreted as representing the momentum components due to buoyancy, turbulence suspension, drag, lift and added mass. Among these, the first three dominate the total interphase momentum exchange in sediment-laden flows, while lift and added-mass forces are generally considered to be of secondary importance and are often neglected [48,93].

Building on this theoretical framework, the general form of the fluid-to-solid interphase momentum exchange per unit volume, as implemented by Cheng et al. [48] in their OpenFOAM-based solver *SedFOAM* and subsequently adopted in other related studies [49,82], can be expressed as:

$$\boldsymbol{M_{fs}} = -\varphi\beta\left(\boldsymbol{u_f} - \boldsymbol{u_s}\right) + \beta\frac{\nu_{ft}}{\sigma_c}\nabla\varphi + \nabla\left[p_f(1-\varphi)\right] \tag{41}$$

where p_f is the fluid pressure, β is a drag parameter, σ_c is the Schmidt number and ν_{ft} is eddy viscosity. The three terms on the right-hand side represent mean drag, turbulent suspension, and buoyancy effects, respectively.

The first term describes the drag force arising from the difference in fluid and solid velocities. Its coefficient β is commonly defined using empirical correlations; numerical scouring studies [48,49,91] typically employ a closure in which β is a function of both φ and particle Reynolds number. Such a closure for β is suitable for both dense and dilute sediment-concentration regimes, as it ensures smooth drag transitions between them. The second term represents the turbulent suspension effect, which captures the momentum transfer resulting from correlations between fluctuations in sediment concentration and fluid velocity. Its formulation involves the turbulent Schmidt number σ_c, a dimensionless parameter that characterises the ratio of turbulent momentum diffusivity to sediment diffusivity. The value of σ_c is expected to vary with particle size, flow regime, and turbulence intensity. Previous studies [107,108] have reported $\sigma_c < 1$, indicating that sediment diffusivity generally exceeds momentum diffusivity in turbulent flows. For simplicity and numerical robustness, Cheng et al. [48] adopted $\sigma_c = 1$, noting that variations in this parameter exert a comparatively minor influence on model stability relative to uncertainties associated with drag closure.

Lift and added-mass forces, not accounted for by Equation (41), become significant in regions where spatial velocity gradients, strong shear, or rapid particle accelerations occur. These effects are particularly relevant under highly unsteady flow conditions, such as impulsive wave impacts or bed collapse events. A more comprehensive formulation of the interphase momentum exchange that explicitly incorporates these additional forces is presented by Mathieu et al. [82].

5.2.4. Fluid Turbulence Closure

Turbulence plays a critical role in scouring phenomena, controlling the entrainment, suspension, and transport of sediment. Within Eulerian–Eulerian two-phase formulations, the representation of turbulence is particularly challenging due to the need to resolve interactions between fluid velocity fluctuations and dispersed sediment particles. Unlike single-phase turbulence models, which are typically calibrated for clear-water flows, two-phase approaches must account for particle-induced turbulence modulation, turbulence-driven sediment suspension, and the fluid–sediment coupling mechanisms.

From Equations (11) and (41), the eddy viscosity and fluid stress require closure. The fluid stress comprises the conventional viscous and Reynolds stresses ($\boldsymbol{R_f}$) together with a grain-scale contribution associated with fluid–particle interactions ($\boldsymbol{r_f}$), the latter being commonly neglected because of limited experimental data [48]. The most widely adopted approach has been the use of Reynolds-Averaged Navier–Stokes (RANS) models, particularly the k-ε [59] or k-ω [60] formulations, where k is turbulent kinetic energy, while ε and ω are turbulent kinetic energy dissipation rates. The two widely adopted definitions of eddy viscosity for the two closures are:

$$\nu_{ft} = C_\mu k^2/\varepsilon \tag{42}$$

$$\nu_{ft} = k/\omega \tag{43}$$

where C_μ is an empirical coefficient.

For sediment-laden scour, conventional k-ε clear-fluid turbulence closures have been modified to account for sediment-induced effects on turbulence [48,49,86,87,94]. The principal modification accounts for turbulence damping caused by density increase, with density gradients significantly attenuating turbulence, particularly for fine sediments at high Shields parameters [74]. A second modification accounts for turbulence modulation associated with drag and particle inertia [109]. Particle inertia additionally governs the degree of fluid–sediment coupling: low-inertia particles tend to follow turbulent fluctuations, whereas larger-inertia particles respond less strongly to eddy motion and may themselves modify the turbulence field.

Hsu et al. [94] proposed a k-ε turbulence closure for sheet-flow conditions involving massive particles, where the accuracy of the turbulence closure is less critical to the model's reliability compared with the granular-flow formulation. Amoudry et al. [86] extended the formulation to improve its applicability to finer sediments, for which turbulence-model selection becomes increasingly important. It should also be noted that, for scour problems with large particles, small-scale turbulence can become important, which, however, is neglected in most of the existing turbulence formulations. These conditions can result in excessive energy dissipation of the flow, which is not captured when small-scale turbulence effects are not considered [94]. Neglecting this mechanism underestimates the total energy dissipation, potentially leading to overpredicted flow velocities under prescribed forcing, or underestimated hydraulic resistance under prescribed discharge. The associated errors in near-bed velocity and shear stress may affect sediment mobilisation and the predicted rate of scour development, even if the final scour depth is less sensitive.

The k-ε turbulence closure is widely used for high-Reynolds-number flows but becomes less reliable near solid boundaries where adverse pressure gradients, flow separation, strong shear, and anisotropic vortex structures occur [49,55,110]. In particular, and as demonstrated by Ikani et al. [55], the k-ε tends to underestimate turbulent kinetic energy in high-shear zones close to the bed or structural surfaces, where complex turbulence generation and dissipation dominate. k-ω-based formulations generally provide improved near-wall behaviour and have therefore been adopted in scour simulations where reliable representation of the near-bed boundary layer is important [110]. Menter [111] combined the k-ω formulation near walls with k-ε-type behaviour away from boundaries through the baseline (BSL) model and subsequently the shear-stress-transport (SST) model. The k-ω SST formulation additionally limits the turbulent viscosity in regions of strong shear, improving the representation of flow separation under adverse pressure gradients [44,76,111,112]. It has consequently been widely adopted in scour simulations [44,81,110,112].

Jha and Bombardelli [113] were among the first to adapt Wilcox's [114] k-ω closure for two-phase dilute sediment-laden flows, adding terms to represent fluid–particle velocity

correlations and drag-induced energy exchange. Amoudry [115] extended this approach for dense oscillatory sheet flows, incorporating an explicit interphase momentum-transfer term that adds dissipation due to drag-related velocity differences between phases. This additional source reduces k and increases ω in regions of strong coupling. Unlike Jha and Bombardelli's [113] dilute-flow formulation, Amoudry's [115] model included granular rheology to capture particle collisions and near-bed stresses, making it more suitable for conditions involving high sediment concentrations and strong phase coupling. Cheng et al. [48] and Chauchat et al. [49] implemented some of the above k-ε and k-ω formulations within the OpenFOAM-based solver, SedFOAM. SedFOAM also incorporates the mixing length turbulence model proposed by Jenkins and Hanes [116], which has been applied mainly to 1D two-phase sheet-flow simulations [117].

While RANS-based closures dominate current two-phase scour modelling, Large Eddy Simulation (LES) is gaining interest for capturing unsteady, anisotropic turbulence and coherent structures, such as horseshoe vortices, ripple-induced vortices, separated shear layers, wake structures, and near-bed streaks associated with downstream sediment transport [118]. LES is based on the classical Smagorinsky [61] formulation and resolves larger energy-containing turbulent structures through the direct numerical simulation (DNS) method and small-scale ones through sub-grid scale stress (SGS) method [54]. This improves turbulence representation but requires fine grids, especially near the bed [81], making LES computationally expensive for large-scale scour simulations. Hybrid RANS–LES models, such as the k-ωSST-IDDES [119] and k-ωSST-SAS [120], balance accuracy and cost by applying RANS treatment near walls and LES in regions where large-scale eddies dominate. These hybrid approaches have shown promise for resolving key unsteady structures in scour flows while maintaining computational feasibility [81], although their application in fully coupled two-phase sediment transport remains limited.

5.2.5. Sediment Transport and Bed Evolution

A distinctive strength of Eulerian–Eulerian models is their ability to resolve sediment transport and bed evolution in a unified continuum framework. Unlike traditional morphodynamic models, which rely on empirical bed-load formulas coupled with the Exner equation, the Eulerian–Eulerian approach treats sediment flux as an emergent property of phase interactions and bed deformation. Bed evolution in two-phase models arises naturally from the conservation of sediment mass and momentum, without requiring separate erosion–deposition source terms. This approach allows for more realistic simulation of transient processes such as avalanching, momentary bed failure, and sheet-flow transport.

Near the bed, the sediment volume fraction may increase to around 60% [49]. Here, particle–particle stresses dominate, and the bed behaves as a quasi-solid with intermittent mobilisation. Cheng et al. [48] demonstrated this in SedFOAM by capturing momentary bed failure events, where horizontal pressure gradients induced by steep waves destabilised the bed and generated bursts of transport that could not be explained by bed shear stress alone. In fact, it was shown that the dimensionless shear stress, the Shields parameter, may become irrelevant in cases of sediment transport due to bed failure. These results highlight the capacity of Eulerian–Eulerian frameworks to move beyond Shields-parameter-based formulations that are commonly used to assess the sediment transport. As mentioned, these frameworks enable the transition from immobile to mobile layers by combining collisional and frictional closures.

Recent studies have also derived scaling relations linking sediment flux to parameters such as the Shields, Reynolds, and Stokes numbers. These laws provide non-dimensional power-law relations linking sediment flux to near-bed turbulence intensity and shear. Keetels et al. [26] demonstrated that sediment flux scales with $Re_p\theta^{1.5}$ at moderate Shields

numbers ($0.15 < \theta < 1$), where buoyancy and turbulence production dominate. It scales with $\theta^{0.5}$ at higher Shields numbers ($\theta > 1$), where TKE dissipation is dominated by collisions and drag and sediment flux becomes less sensitive to θ. This transition highlights the role of turbulence modulation, rather than mean shear alone, in dense sediment entrainment and provides a physically grounded link between empirical transport formulations and two-phase turbulence-resolving models.

Two-phase models have also demonstrated the capability to resolve phase-dependent transport processes without empirical partitioning between bed-load and suspension. Salimi-Tarazouj et al. [121] applied SedFOAM to investigate wave-shape asymmetry and skewness, showing that these characteristics strongly influence phase-lag effects and sediment-transport direction. Acceleration-skewed waves produced predominantly onshore transport, and velocity-skewed waves produced offshore transport, while combined asymmetry and skewness resulted in competing mechanisms and reduced net transport.

Nagel et al. [45] reproduced live-bed scour around a vertical pile, including upstream horseshoe-vortex scour and wake deposition. Importantly, the model captured gravitational avalanching of sediments when the bed slope exceeded the angle of repose, a process usually parameterised empirically in classical morphodynamic models. Applications to scour downstream of aprons [49] and beneath pipelines [122,123] further illustrate the value of this approach. More recently, the two-phase approach was extended to a three-phase model and implemented in a new OpenFOAM solver, sedInterFOAM, to account for free-surface effects on sediment-transport problems [82]. These advances underline the potential of Eulerian–Eulerian models to reveal mechanisms of bed instability and sediment mobilisation that remain hidden in conventional formulations.

5.2.6. Numerical Implementation in Finite-Volume Method

The algorithmic structure of Eulerian–Eulerian two-phase scour models is summarised in Figure 4, which illustrates the exchange of information between the CFD solver, the granular-stress closure and the interphase interaction closure over a single time step. Eulerian–Eulerian two-phase models are commonly implemented within finite-volume frameworks such as OpenFOAM [48,49,82,122] and FLOW-3D [124,125]. OpenFOAM has gained wider adoption for scour-related simulations due to its open-source accessibility and flexibility for developing customised multiphase solvers. Several two-phase solvers, including SedFOAM [48], SedFOAM-2.0 [49] and SedInterFOAM [82], employ collocated grids with Rhie–Chow interpolation to prevent pressure–velocity decoupling [126]. In OpenFOAM, this correction is embedded in the SIMPLE, PISO, and PIMPLE pressure–velocity coupling algorithms.

Pressure–velocity coupling is commonly handled using PISO or PIMPLE for transient scour simulations. PISO is directly formulated for transient calculations, while PIMPLE combines PISO-type corrections with outer iterations, providing additional robustness for strongly coupled problems and allowing the selection of greater time steps [127]. The time step is constrained by the Courant number, which is typically kept below unity and defined as the product of local cell velocity ($\boldsymbol{U}$) and the time step (Δt) divided by the cell distance (Δx), as shown in Equation (44). PIMPLE provides both robustness and temporal reliability and has therefore been widely adopted in unsteady two-phase sediment-transport and scour simulations [48].

$$Co = \boldsymbol{U}\Delta t/\Delta x \tag{44}$$

In the solver of Cheng et al. [48], the momentum equations for both phases are first solved to obtain intermediate velocities, with interphase drag evaluated explicitly from the previous time step. A pressure equation is then derived from the phase continuity equations

and used to correct the velocities of both phases. The corrected velocities are subsequently used to update the sediment concentration, turbulence variables, and phase stresses.

Mesh design plays a crucial role in resolving bed–flow interactions. Adequate mesh resolution is required near the sediment bed and around structures to capture steep concentration gradients and scour-driving vortices [45]. Time stepping should also satisfy Courant–Friedrichs–Lewy (CFL) constraints associated with both fluid and relative fluid–sediment fluxes [49]. These requirements can impose small time steps, particularly in three-dimensional simulations with high sediment concentrations, increasing computational cost.

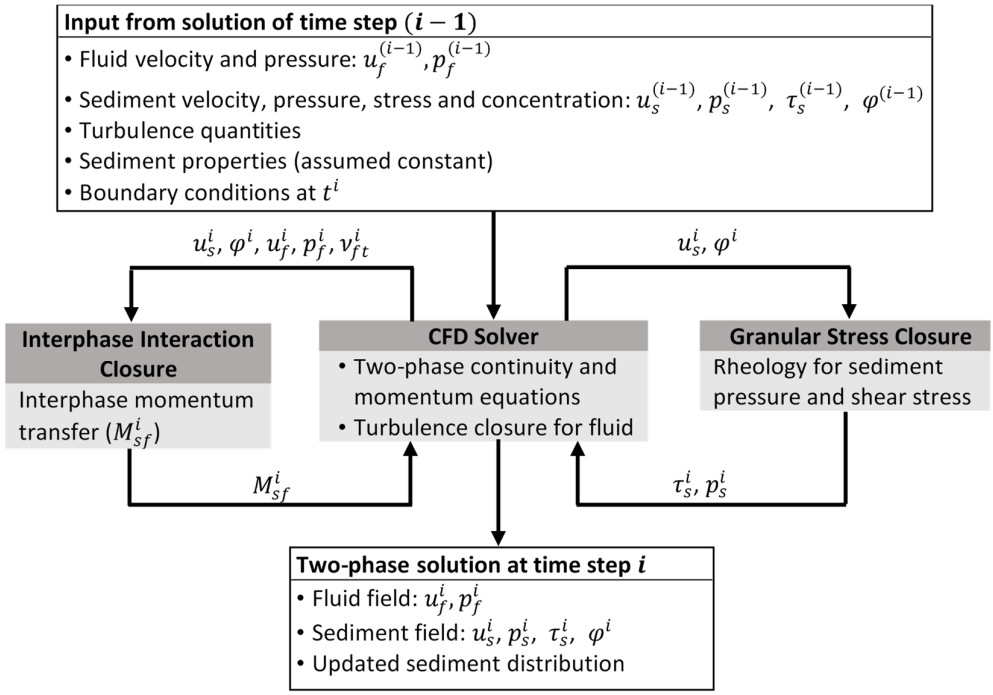


Figure 4. Schematic information exchange between two-phase CFD solver, granular-stress and interphase interaction closures within a single time step i.

5.2.7. Advantages and Limitations

Eulerian–Eulerian two-phase models can represent both dense near-bed layers and dilute suspensions within a unified framework, without empirical partitioning between bed load and suspended load. Sediment transport emerges from the coupled conservation equations, allowing entrainment, sheet flow, avalanching, and suspension to be examined within a unified framework. The approach also accounts for two-way feedback between sediment and turbulent flow, which is important under strongly coupled scour conditions.

However, these capabilities come at substantial computational cost, mainly because of the fine near-bed resolution and small time steps imposed by CFL restrictions [45]. Computational demands increase further for three-dimensional simulations and strongly coupled sediment–flow conditions, limiting feasible domain size and simulation duration. For this reason, they are mostly validated against experimental data, while their extension to field conditions remains uncertain, particularly for heterogeneous sediments, stratified flows, or irregular wave climates. Model reliability also depends strongly on the closures used for granular stresses, turbulence, and turbulence–sediment coupling. Their applicability depends on sediment characteristics and flow conditions, and reliability may decrease when closures are applied outside the conditions for which they were calibrated. Many turbulence-model coefficients are based primarily on clear-fluid data and remain insufficiently validated across different grain sizes, concentrations, and stratification con-

ditions [49,94]. Additionally, the commonly used turbulence closures neglect small-scale turbulent motions, potentially underestimating flow-energy dissipation, particularly for relatively large sediment particles [94].

Turbulence-model selection therefore involves a trade-off between near-bed resolution and computational cost. Low-Reynolds-number formulations (e.g., k-ωSST) require very fine near-wall meshes which increase computational demand and may hinder numerical convergence, whereas wall-function approaches (e.g., k-ε) permit coarser resolution but may introduce near-bed velocity bias [110]. More advanced approaches such as Reynolds-stress models and LES can better represent complex unsteady turbulence but substantially increase computational cost [55]. Moreover, this additional cost may not always result in significant improvement over less computationally demanding k-ωSST and k-ε formulations [110].

5.2.8. Engineering Applicability

Two-phase Eulerian–Eulerian CFD models are particularly suitable for problems involving dense sediment transport, sheet-flow conditions, live-bed scour, and cases in which feedback between sediment concentration, turbulence, and flow momentum is important. Their applicability is more limited for routine design or large field-scale parametric studies, unless sufficient computational resources and appropriate calibration data are available. The principal engineering limitation of two-phase Eulerian–Eulerian models is their sensitivity to granular-stress closures, turbulence–sediment coupling assumptions, and near-bed resolution.

6. CFD–DEM

The coupling of Computational Fluid Dynamics (CFD) with the Discrete Element Method (DEM) has become an influential tool for investigating sediment transport and scour, enabling simultaneous resolution of fluid dynamics and particle-scale mechanics. CFD–DEM adopts a Eulerian–Lagrangian strategy wherein the fluid is solved in the Eulerian domain and each sediment grain is tracked explicitly in the Lagrangian domain. Unlike continuum approaches, this framework permits direct representation of particle collisions, microstructural rearrangements, and fluid–structure interaction, all of which are central to the initiation and development of scour.

6.1. Fluid Phase

The carrier fluid in CFD–DEM models is governed by the incompressible Navier–Stokes equations, formulated to incorporate the influence of sediment particles. The resulting mass and momentum conservation equations (Equations (19) and (21)) are structurally identical to those used in the Eulerian–Eulerian formulation presented in Section 5.2.1. However, the physical interpretation differs substantially. In CFD–DEM, the local sediment concentration is not obtained from a continuum transport equation but is instead computed directly from the spatial distribution of DEM particles within each CFD control volume, providing an instantaneous, geometry-based estimate of porosity.

Similarly, although the fluid momentum equation includes the same interphase momentum-exchange terms—drag, lift, pressure-gradient, and viscous forces—their computation differs between the two frameworks. In CFD–DEM models, these forces are evaluated explicitly for each individual particle and subsequently mapped onto the fluid mesh as volumetric source terms. This approach is more rigorous than that used in Eulerian–Eulerian models, which rely on continuum closures for interphase momentum exchange, typically based on empirical drag correlations and constitutive assumptions for multiphase flow. Turbulence modelling also follows a distinct practice in CFD–DEM simulations. Be-

cause resolving the large-scale coherent structures that drive sediment entrainment is often crucial, Large Eddy Simulation is the preferred choice [25,54]. Nevertheless, RANS closures have also been employed [110] in studies where computational efficiency is a priority.

6.2. Particle Phase—DEM

In the DEM formulation, sediment grains are treated as discrete spherical entities subjected to various forces all acting at their centre due to particle–particle and particle–fluid interactions. The forces acting on each particle include normal contact (f_n), tangential contact (f_t), gravity, and fluid–particle forces. The latter consist of the drag (f_d), pressure gradient (f_p) and viscous forces (f_v), the definitions of which can be found in [25]. By taking the equilibrium of these forces for each particle i and complying with Newton's second law, the equations that govern the particle's translational and rotational motion are respectively given by:

$$m_p \frac{d\boldsymbol{u}_{p,i}}{dt} = \sum_{j=1}^{n_c} \left(\boldsymbol{f}_{n,ij} + \boldsymbol{f}_{t,ij} \right) + m_p \boldsymbol{g} + \boldsymbol{f}_{d,i} + \boldsymbol{f}_{p,i} + \boldsymbol{f}_{v,i} \tag{45}$$

$$I_p \frac{d\boldsymbol{\omega}_{p,i}}{dt} = \sum_{j=1}^{n_c} \left[\boldsymbol{R}_i \times \left(\boldsymbol{f}_{n,ij} + \boldsymbol{f}_{t,ij} \right) \right] \tag{46}$$

where $\boldsymbol{u}_{p,i}$ and $\boldsymbol{\omega}_{p,i}$ are the particle's translational and angular velocities, m_p and I_p are the particle's mass and rotational inertia, $\boldsymbol{g}$ is the gravity vector, $\boldsymbol{R}_i$ is the vector from the contact point to the particle's centre, and n_c is the number of particles that are in contact with particle i.

The normal and tangential contact forces are computed using a particle–particle contact model. The Hertz–Mindlin non-slip model [128] is typically used in CFD–DEM scour simulations [25,54,110], which prescribes normal and tangential spring–dashpot behaviour, and slipper based on Coulomb friction limits. The normal contact force can be defined either through a linear elastic model or through a more advanced nonlinear formulation. While linear elastic models are simple and computationally efficient, their reliability relies on the model's elastic parameters, which are often difficult to determine, and they do not adequately capture the evolving force–displacement behaviour typical of granular systems. In sediment transport, where particle contacts experience rapidly varying loads, such limitations become significant. For this reason, Yazdanfar et al. [110] adopted a nonlinear Hertz–Mindlin contact model, as it provides a more realistic representation of collision mechanics and better reflects the dynamic nature of particle interactions.

6.3. Numerical Coupling

CFD–DEM models rely on a bidirectional exchange of information between the Eulerian fluid field and the Lagrangian particle system. Figure 5 schematically illustrates the CFD–DEM numerical coupling procedure, highlighting the exchange of flow variables, particle kinematics, and interaction forces between the CFD solver, the DEM solver, and a coupling routine within a single physical time step. The figure also indicates the iterative nature of the coupling, which continues until convergence is reached before advancing to the subsequent time step.

Previous scour-related CFD–DEM studies employ the *CFDEMcoupling* framework originally developed by Goniva et al. [129], which links the finite-volume CFD solver OpenFOAM with the DEM package LIGGGHTS. In this framework, the coupling proceeds as follows [25]: the CFD solver first updates the fluid flow field and passes pressure, velocity, and eddy viscosity data to the coupling routine. Using these fields, the coupling module computes the hydrodynamic forces acting on individual particles $\left(f_d^i,\ f_p^i,\ f_v^i \right)$ and supplies them to the DEM solver. DEM then assembles all resultant forces on each particle

and updates the particle positions and velocities. This information is fed into the coupling routine, which solves the particle-scale momentum equations and calculates the resulting particle concentration and fluid–particle interaction forces in each CFD cell. These updated particle fields are transferred back to the CFD solver, where they are used as source terms or porosity fields in the fluid momentum equations. The CFD solver then updates the flow field for the next time step, completing the two-way coupling cycle. The time step update is different for each framework. In particular, DEM requires a time step small enough to resolve the collision time, typically orders of magnitude smaller than the fluid time step [25,110].

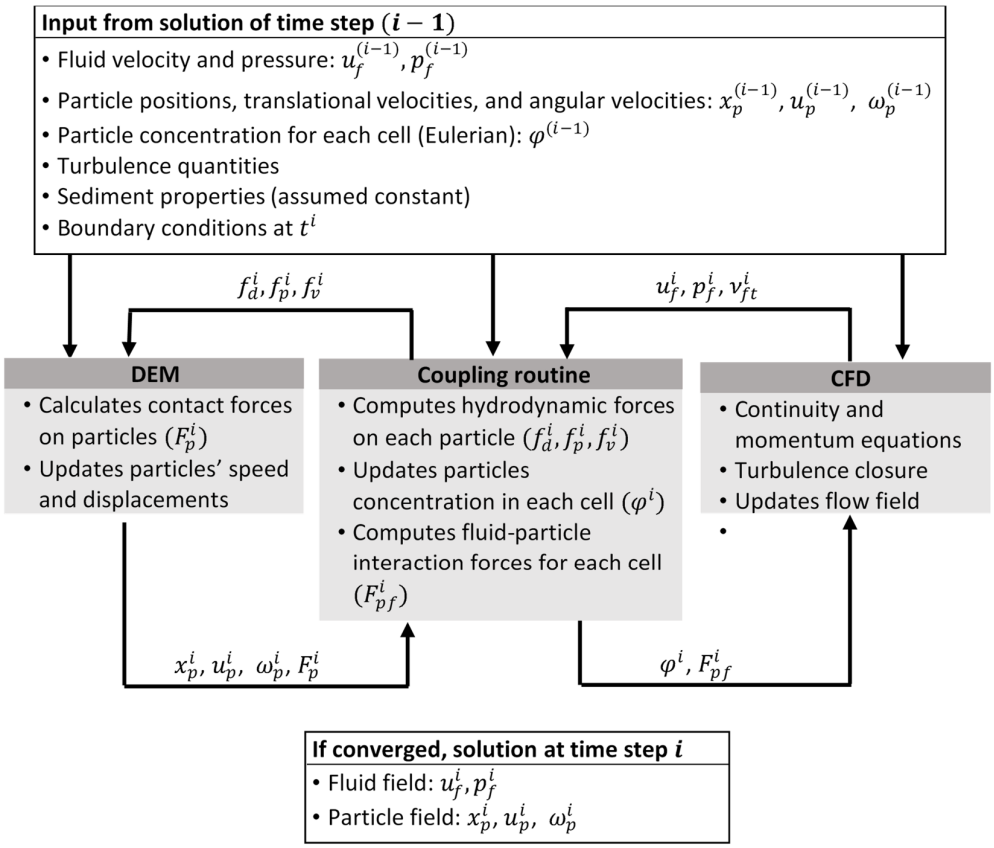


Figure 5. Schematic information exchange between CFD and DEM solvers within a single time step i.

This procedure inherently accumulates the particle-level interaction forces at the CFD-cell level rather than treating them as independent local force evaluations. Equation (45), by contrast, defines the force balance of each individual DEM particle. When a macroscopic structural load is required, such as for evaluating the nonlinear loading response of a deep foundation, the relevant local force contributions must subsequently be summed over the full region of interest; this may be performed over successive depth intervals and cumulatively integrated to obtain the total resultant force. This global force evaluation is therefore distinct from, but consistent with, both the particle-level force balance and the particle-to-cell force-transfer procedure used in CFD–DEM coupling.

Spatial resolution poses a major challenge in CFD–DEM coupling. In principle, the most physically rigorous approach is the resolved CFD–DEM method, in which the fluid mesh is refined to a scale smaller than the particle diameter, allowing the flow around each particle to be explicitly resolved. Although this approach yields highly reliable hydrodynamic forces, it is prohibitively expensive and therefore impractical for scour simulations. Consequently, scour studies adopt the unresolved CFD–DEM strategy, where CFD-cell sizes are significantly larger than the particle diameter. In this framework, particle prop-

erties computed by DEM are averaged over the CFD control volume, and hydrodynamic forces are computed using empirical correlations rather than fully resolved flow fields. While computationally feasible, this scale separation limits the achievable resolution near the sediment bed, where steep gradients in shear stress and porosity are critical. The insufficient near-wall resolution generally necessitates the use of wall functions, which introduce additional modelling assumptions and may reduce the accuracy of predicted boundary-layer dynamics [54].

6.4. Model Acceleration and Upscaling

To mitigate the computational demands arising from the large number of simulated particles, the coarse grain method has been adopted in the DEM framework of CFD–DEM coupled scour simulations [25,54,130]. This method replaces clusters of particles with larger particles, whose forces represent the accumulated forces of the enclosed particles. Takabatake et al. [131] outlined three key assumptions underlying the coarse-graining strategy. First, the motion of each coarse particle—its displacement and velocity—is taken to represent the averaged behaviour of the original group of finer particles. Second, the contact forces applied to a coarse particle are determined by enforcing equivalence of kinetic energy between the coarse-grained system and the underlying real-particle system. Third, a collision between two coarse particles is treated as representing the simultaneous impact of all constituent real particles that the coarse particle represents. This approach offers substantially reduced computational needs but requires careful treatment to avoid distortion of sediment-transport rates or bed geometry. Ma et al. [25] found that results are stable when the coarse particle to real particle diameter ratio is two or smaller. The same authors highlighted the need for a scaling correction to preserve dynamic similarity, typically by adjusting the gravitational acceleration or, equivalently, the Shields number to compensate for the artificially increased particle size.

Yazdanfar et al. [110] introduced an alternative upscaling framework for mitigating the computational demand of the method. The framework links detailed microscale CFD–DEM simulations to a computationally efficient macroscopic CFD model. The key idea is to perform microscale high-fidelity CFD–DEM simulations in an idealised, statistically homogeneous turbulent flow using sediment particles identical in size and shape to those in the target large-scale problem. These microscale simulations provide detailed information on particle impacts, near-bed turbulence, and sediment mobilisation that would be prohibitively expensive to resolve directly at engineering scales. Rather than resolving particle mechanics across the full macroscopic domain, the method uses the microscale results to construct a *scour function*—a reduced-order relation that links local-scour rate to key hydrodynamic and particle-scale variables. This function is then embedded within a conventional CFD model, enabling the bed morphology to evolve without invoking DEM at the large scale.

The microscale stage requires a suite of CFD–DEM simulations that cover a range of Reynolds numbers and suspended-sediment concentrations, from clear-water to live-bed regimes, to capture how particle impacts and bed responses vary under different turbulence intensities. These microscale simulations are run over long durations to obtain a sufficient statistical sample and create a reliable probabilistic scour model. This model, which is embedded in the scour function, relates scour rate to local fluid shear stress and the kinetic energy of particles impacting the bed. In the macroscopic application, only the suspended sediment is explicitly tracked using a standard CFD method, while the dense sediment bed is not resolved. Instead, the bed is treated as a boundary that evolves according to the local-scour rate obtained from the scour function. When the computed change in local bed

elevation exceeds a threshold, the CFD mesh is updated accordingly, and the simulation continues with the revised morphology.

By eliminating DEM from the large-scale phase—where it is most computationally expensive—the method reduces both memory requirements and CPU cost by orders of magnitude. While the present formulation is tuned to flows approximating homogeneous, wall-bounded turbulence, the conceptual framework has the potential to be extended to flows dominated by coherent flow structures, such as horseshoe and lee vortices around hydraulic structures. However, such extensions require further validation and refinement.

6.5. Advantages and Limitations

CFD–DEM explicitly represents particle motion through particle–particle and particle–fluid forces, avoiding the empirical sediment-transport formulas and granular-stress closures required by continuum approaches. This enables direct representation of grain-scale processes such as collisions, frictional contacts, and rolling [130]. By tracking individual grains, CFD–DEM also provides information on particle trajectories and local force balances relevant to sediment entrainment. Ma et al. [25], for example, showed that increasing the Shields parameter increased both the number of mobilised grains and scour depth around a monopile. CFD–DEM can also represent seepage-related forces within the sediment bed and vertical drag forces that contribute to the onset of particle instabilities. For example, Zhang et al. [54] showed that upward seepage reduces the effective particle weight and promotes erosion by increasing the drag–gravity ratio. Furthermore, CFD–DEM has been used to identify the flow pathways and sediment-transport patterns that govern the progression of local scour, providing valuable mechanistic insight into processes such as toe erosion, slope destabilisation, and sediment redeposition [25,54].

The principal limitation of CFD–DEM is its high computational cost, arising from the small DEM time steps and large particle numbers required. These requirements restrict the feasible domain size and simulation duration even when coarse-graining strategies are employed. The upscaling framework proposed by Yazdanfar et al. [110] reduces computational demand by embedding microscale CFD–DEM information within a conventional CFD model, although further validation is required. A further limitation of unresolved CFD–DEM is that CFD cells must remain larger than the sediment particles, constraining fluid-field resolution near boundaries [110]. This may limit resolution of important flow structures, such as the horseshoe vortex at a pile base. In addition, most studies employ spherical, monodisperse particles, neglecting grain shape, angularity, and grading, all of which can strongly influence sediment mobility and packing behaviour [132]. Model reliability also depends on appropriate calibration of the particle-contact laws.

6.6. Engineering Applicability

CFD–DEM models are particularly suitable for mechanism-focused studies of incipient sediment motion, avalanching, seepage-induced instability, particle-contact behaviour, and local-scour processes at relatively small spatial scales. At present, CFD–DEM is not feasible for direct field-scale design because of its high computational demands, but it provides grain-scale insight that can support the development, calibration, and validation of continuum closures or reduced-order engineering models. Therefore, CFD–DEM should generally be regarded as a high-fidelity research and model-development tool rather than a routine design method for full-scale marine infrastructure.

7. Smoothed Particle Hydrodynamics

Smoothed Particle Hydrodynamics (SPH) was first introduced by Gingold and Monaghan [133] for astrophysical simulations, but it has since been widely adopted in fluid

mechanics, including sediment-transport and scour modelling. Unlike mesh-based CFD methods, SPH is a fully Lagrangian, mesh-free formulation in which both fluid and sediment phases are represented by moving particles. This characteristic allows the method to handle large deformations of the free surface, sharp morphological changes in the bed, and the formation of steep or irregular scour pits—scenarios that pose significant challenges to mesh-dependent finite-volume solvers. In scour modelling, SPH has been used either as (i) a single-phase fluid solver coupled with a DEM solver for particle motion (SPH–DEM), or (ii) a multiphase continuum approach in which both fluid and sediment are treated as SPH phases with their own rheological properties. The method has been employed across a broad range of applications, including local scour around bridge piers [50,134], caisson breakwaters [135], vertical breakwaters [136], and reservoir sediment flushing [137].

7.1. Discretisation of Governing Equations

Within the SPH framework, particle motion is fundamentally governed by the N-S equations, which describe the conservation of mass and momentum for viscous flows. However, given the discrete nature of particles, these continuous partial differential equations must be transformed into discrete form to properly accommodate the individual particle positions [50]. This is achieved using a kernel function, which distributes particle properties over a spatial distance, referred to as the smoothing length, and approximates spatial derivatives from neighbouring particles. As a result, particle properties, including mass, density, velocity, pressure, and their derivatives, can be evaluated in discrete form while allowing each particle to interact with its surrounding particles.

7.2. Irregular Particle Spacing and Stabilisation in SPH

A numerical issue in SPH analyses is the development of non-uniform particle distributions, particularly in highly turbulent flows. Such irregular spacing can cause the smoothing kernel to introduce artificial high-frequency noise in the computed velocity and pressure fields. To mitigate this issue, Zhang et al. [50] adopt the particle-shifting technique originally proposed by Lind et al. [138]. In this approach, fluid and mobile sediment particles are subjected to a small corrective displacement at each time step to re-establish a more uniform spatial arrangement. The displacement for each particle is determined by assessing the kernel-weighted contribution of its neighbours and is capped—typically to less than one-fifth of the smoothing length—to prevent excessive correction that might distort physical motion.

7.3. Fluid Phase

In the SPH representation, the fluid domain is discretised into particles that carry mass, velocity, pressure, and other physical properties. Particle velocities are estimated by solving the N-S equations. Turbulence modelling in SPH is most commonly handled through LES to solve turbulent structures that occur at sub-particle scales. For the estimation of the pressure-gradient term incorporated in the momentum conservation equation, the fluid is treated as either incompressible or weakly compressible.

Although less accurate, the weakly compressible SPH (WCSPH) method is simpler to implement and provides faster solutions per time step. As implemented by Zhang et al. [50,137], the equation of state (EOS) is required to relate fluid pressure and density before the pressure gradient is expressed in discrete form. This introduces small fluctuations in fluid density, which should be controlled so that they remain within reasonable limits that do not compromise mass conservation. However, particles located near the fluid–sediment interface often exhibit pronounced density oscillations because of the large contrast in material densities. As noted by Wang et al. [139], when particles of markedly different density or mass exist within the smoothing length, the kernel function can yield unreliable

estimates of density and pressure. These numerical inaccuracies appear as artificial pressure gradients, which may result in spurious surface-tension forces and numerical instabilities. To mitigate this issue, Zhang et al. [50] suggest using the δ-SPH model proposed by Antuono et al. [140].

To eliminate the intrinsic numerical challenges associated with the WCSPH formulation, Wang et al. [134] suggest the use of the incompressible SPH (ISPH) method. Unlike WCSPH, which allows for weak compressibility of the fluid and small artificial density fluctuations, ISPH imposes incompressibility explicitly through a projection-based pressure–velocity coupling procedure. At each time step, the flow solution is split into two sub-steps. First, a provisional particle velocity field is obtained without enforcing incompressibility, using only viscous and external forces. In the second sub-step, a pressure Poisson equation (PPE) is solved to determine a pressure field that corrects the provisional velocities, ensuring that the final velocity field complies with the incompressibility condition. The PPE is discretised using the SPH kernel and solved iteratively, and the resulting pressure gradient is then used to update particle velocities and positions. This approach eliminates density oscillations and suppresses spurious pressure fluctuations that commonly arise in WCSPH as a result of its quasi-compressible treatment of the flow. However, the need to solve a global pressure Poisson equation at every time step makes ISPH more expensive than WCSPH, especially in large three-dimensional domains. Despite this overhead, Wang et al. [134] demonstrate that the improved stability, reduced numerical dissipation, and higher fidelity in pressure and velocity fields make ISPH a robust alternative for simulating sediment mobilisation and bed evolution around hydraulic structures.

7.4. Sediment Model

The sediment phase in SPH scour simulations is represented using either a continuum SPH sediment phase or a DEM approach.

7.4.1. Continuum Sediment Modelling

In continuum-based SPH models, the sediment phase is also governed by the N-S equations together with a constitutive law that reflects its non-Newtonian behaviour. This continuous representation of sediment offers greater computational flexibility than DEM where particles explicitly represent grains. Zhang et al. [50,137], for example, employed the Herschel–Bulkley–Papanastasiou (HBP) model [141], which represents quasi-solid behaviour below yielding and highly viscous flow after yielding. This transition is typically governed by a soil-mechanics failure criterion, such as the Drucker–Prager [50,137] or the Mohr–Coulomb [134].

Because the yield criterion is evaluated from the mechanical state of individual SPH sediment particles, the spatial extent of the yielded region can also be reconstructed from particle-level results. Particles satisfying the adopted failure criterion can be identified and visualised directly or spatially interpolated to generate two-dimensional contours or three-dimensional isosurfaces. Similar approaches have been employed in SPH geomechanics to identify failure surfaces from spatial distributions of accumulated plastic strain [142], while Zubeldia et al. [143] demonstrated the spatial identification of yielded and unyielded sediment regions in an SPH erosion model using the Drucker–Prager criterion. Such post-processing therefore enables the evolution of internally yielded sediment zones to be examined despite the absence of a fixed computational mesh.

While the yield criterion governs the internal mechanical response of the sediment below seabed, entrainment of surface particles requires an additional hydrodynamic condition. The Shields criterion is commonly applied, with motion initiated when the local bed shear stress exceeds a slope-corrected critical value (e.g., Equations (2) and (3)). Within

SPH, local bed slope and shear stress are estimated from neighbouring particles using kernel-based interpolation [50]. Once the Shields threshold is exceeded, a sediment particle enters the bed-load state and follows the prescribed HBP rheology. If its uplift velocity exceeds a critical value, it is reclassified as suspended sediment and treated as a Newtonian phase, for example, using the Vand [144] viscosity model [50,137]. When its normal settling velocity falls below the prescribed threshold, the particle returns to the bed-load state and the HBP rheology is restored. The definitions of uplift and settling critical velocities can be found in [50].

Wang et al. [134] proposed an alternative continuum approach that does not employ an explicit sediment rheology; instead, sediment motion is determined using a slope-corrected Shields criterion based on [145]. Once entrained, a sediment particle becomes a transported water–sediment mixture particle (TWP) with a density that reflects the local mixture. The TWP then evolves under the Navier–Stokes equations, with density updated at each time step as mixing occurs. This formulation does not resolve internal sediment deformation, but it provides a simpler and computationally efficient treatment of sediment initiation and early-stage scour.

Regardless of whether a rheological or non-rheological approach is used, the motion of eroded sediment particles is governed by the particle-level momentum equation, which can incorporate seepage effects. Wu et al. [146] incorporated a seepage-induced drag force, based on the relative motion of pore water and sediment, directly into the SPH momentum equation.

7.4.2. DEM Sediment Modelling

The sediment motion in the SPH–DEM framework is governed by the DEM formulation described in Section 6.2. At each coupling step, the DEM solver receives from the SPH fluid solver the following information:

i. The local porosity, which iscomputed from the previous time step as the complement of sediment concentration.
ii. Interpolated fluid fields, including the fluid velocity, pressure, and their gradients at the position of each DEM particle. These quantities are obtained through kernel-based interpolation within the SPH support domain.

Using this information, DEM evaluates the fluid–particle interaction forces, typically including drag, buoyancy, pressure-gradient, and added-mass contributions. These forces are introduced into Newton's second law to update the translational and rotational motion of each sediment particle.

After the DEM solver advances particle positions and velocities, it passes back to the SPH solver two key pieces of information:

i. The solid volume distribution, from which SPH recomputes porosity for the next fluid step;
ii. The reaction fluid–particle interaction forces, which appear as a momentum-exchange source term in the SPH momentum equation.

This two-way exchange ensures consistent coupling between the fluid and granular phases, allowing the SPH solver to update the fluid field based on the new sediment configuration, while DEM simultaneously evolves particle motion in response to the fluid dynamics.

7.5. Advantages and Limitations

SPH offers several distinct advantages over classical Eulerian and Eulerian–Lagrangian approaches for modelling sediment transport and local scour. These strengths arise primarily from its Lagrangian, mesh-free formulation, which is particularly well-suited to

free-surface flows, and highly deformable multiphase interfaces [134,139]. SPH can also accommodate large morphological changes without the mesh distortion or remeshing required by grid-based approaches [137]. It is therefore particularly advantageous for scour problems involving rapid bed evolution, steep eroded slopes, sediment avalanching, and collapsing cavities, which can be difficult to resolve using mesh-based methods without frequent remeshing or very fine grids.

A key requirement in scour prediction is the reliable identification of the evolving bed surface, which determines the remaining embedment and stability of a foundation. SPH represents the sediment as discrete particles whose states (static, bed-load, or suspended) can be explicitly tracked, enabling reconstruction of the uneroded bed surface by filtering out particles that have transitioned to mobile states [50]. This provides a more robust numerical characterisation of the scoured morphology than Eulerian approaches, where distinguishing genuinely stationary sediment from temporarily resting material within the mobile layer can be challenging [50]. In SPH sediment models, entrainment criteria such as the Shields parameter or slope-corrected incipient-motion formulations can be applied at the SPH-particle level. This eliminates the spatial averaging inherent in Eulerian sediment-transport modules and improves the prediction of the onset of motion and the transitions between static sediment, bed load, and suspended load [50].

In SPH–DEM coupled formulations, sediment is represented by DEM particles, enabling explicit treatment of particle–particle and particle–fluid interactions, as explained in Section 6.5. This capability provides a more realistic representation of granular mechanics than continuum-based sediment models, as demonstrated by Yeganeh-Bakhtiary et al. [136], who applied a two-phase WCSPH–DEM model to standing-wave-induced scour in front of a vertical breakwater and reproduced the measured maximum scour depth and sediment mobilisation and redeposition. An additional strength of SPH–DEM coupling is its ability to represent the motion and failure of solid structures [50]. Iwamoto et al. [135], for example, modelled a caisson breakwater using bonded DEM particles and captured its tilting and displacement following foundation erosion under tsunami loading, demonstrating the potential of SPH–DEM for coupled fluid–soil–structure interaction problems.

Despite its advantages, SPH is computationally demanding because spatial resolution depends directly on particle spacing and small time steps are required, particularly in weakly compressible SPH and SPH–DEM simulations [139]. In addition, turbulence in SPH is commonly modelled using LES-type formulations, rather than the more computationally efficient RANS closures widely used in Eulerian CFD. Turbulence modelling is also less mature, with sub-particle-scale LES formulations remaining less extensively validated for coherent scour-related structures [134]. Model reliability is sensitive to particle spacing, which controls both resolution and computational cost [137]. In coupled SPH–DEM models, compatibility between SPH and DEM resolutions may impose additional constraints. For example, Iwamoto et al. [135] used a DEM particle size equal to the SPH-particle spacing to facilitate fluid–structure force transfer, which can require fine resolution throughout the domain. This dependence on globally consistent particle resolution represents a notable drawback relative to Eulerian CFD, where grid refinement can be applied selectively without constraining the discretisation of solid bodies.

Another drawback of SPH is that the kernel smoothing function can produce unphysical density and pressure estimates when particles with markedly different properties coexist within the smoothing length, as commonly occurs at water–sediment interfaces. This may generate spurious surface-tension effects and numerical instabilities [139]. Stabilisation techniques, such as δ-SPH correction [50] and filtering or regularisation procedures [139], can improve stability but increase algorithmic complexity and computational cost, and may not entirely eliminate spurious oscillations.

7.6. Engineering Applicability

SPH is particularly suitable for research-scale scour problems involving large bed deformation, complex free-surface motion, sediment collapse, and rapid morphological change, where mesh distortion would be severe in grid-based methods. Representative applications include laboratory-scale or local-domain simulations of tsunami-induced scour and rapidly evolving scour holes. SPH–DEM is more appropriate when these conditions are combined with explicit granular mechanics or structural motion, such as scour accompanied by caisson displacement or failure. Both approaches remain less suitable for routine full-scale or long-duration engineering simulations because of their high computational cost and limited field-scale validation.

8. Comparative Synthesis of Modelling Approaches

The preceding sections reviewed single-phase (Eulerian) CFD, two-phase (Eulerian–Eulerian) CFD, CFD–DEM (Eulerian–Lagrangian), SPH (Lagrangian), and SPH–DEM (Lagrangian–Lagrangian) approaches for scour modelling. This section provides a comparative assessment of these methods in terms of their underlying assumptions, applicability, validation status, computational requirements, and practical limitations. The aim is to support model selection according to the intended application, required physical resolution, available data, and problem scale.

8.1. Comparative Interpretation of Method Trade-Offs

Single-phase Eulerian morphodynamic models remain the most computationally efficient approach, making them suitable for large-scale, long-duration, and parametric scour simulations. They perform best where sediment concentrations remain sufficiently low for sediment–flow feedback to be neglected [18,49]. Their main limitation is their strong sensitivity to the selected empirical transport formulation, which can lead to markedly different predictions under the same flow conditions [35]. They are also unable to represent dense sediment transport and strong two-way sediment–flow coupling explicitly [49].

Two-phase Eulerian–Eulerian models offer a more physically grounded representation of sediment–fluid interaction. They can capture the two-way feedback between sediment and turbulent flow, making them better suited to dense sheet flow and energetic flow conditions. Their reliability, however, depends strongly on sediment rheology closures, turbulence modulation formulations, turbulence–sediment coupling, and interphase drag correlations. Predictions may become less reliable when these closures are applied outside the conditions for which they were calibrated. In addition, these models remain computationally demanding for complex 3D scour geometries [45].

CFD–DEM provides the greatest grain-scale resolution among the reviewed CFD-based approaches and is particularly valuable for investigating incipient motion, particle contacts, avalanching, and seepage-related mechanisms [25,54]. Its computational cost and unresolved CFD-cell-size requirements, however, restrict current applications mainly to small-scale, mechanism-focused studies rather than engineering-scale prediction. The cell-size constraint can also limit resolution of important flow structures, such as the horseshoe vortex at a pile base, because the CFD mesh cannot be refined below the scale imposed by the sediment particles [110].

SPH is advantageous for problems involving complex free-surface motion, large bed deformation [139], and moving boundaries, where mesh-based approaches may require substantial remeshing [137]. Unlike Eulerian formulations, SPH can also explicitly track the immobile bed and facilitates determination of the evolving scour geometry [50]. This makes it particularly well-suited for problems in which precise determination of the remaining embedment of a foundation is critical. SPH–DEM extends these capabilities to explicit

granular mechanics and structural motion [50]. Unlike conventional Eulerian–Eulerian scour models, where structures are typically treated as fixed boundaries, SPH–DEM can represent structural displacement and failure during scour [50]. This makes it particularly useful for problems requiring coupled assessment of scour evolution and structural stability. However, compared with Eulerian CFD, SPH-based approaches generally require greater computational effort at comparable resolution, while their turbulence modelling is less mature and less extensively validated [134].

Table 1 summarises the main characteristics of the reviewed modelling approaches, including their fluid and sediment representations, principal constraints, and typical domains of application. Figure 6 provides a qualitative positioning of the five modelling approaches in terms of computational cost, grain-scale resolution, scale of application, and reliance on empirical formulations, highlighting the trade-offs between physical detail and practicality for scour simulations. As indicated by Table 1 and Figure 6, the feasible computational-domain size varies substantially between modelling approaches. Single-phase Eulerian models are the most scalable, whereas two-phase CFD and particularly CFD–DEM and SPH-based approaches are increasingly restricted to smaller domains by their computational requirements. Consequently, many high-fidelity local-scour simulations remain limited to laboratory-scale configurations, which may not fully capture far-field hydrodynamics, sediment supply and other interactions relevant to field-scale conditions.

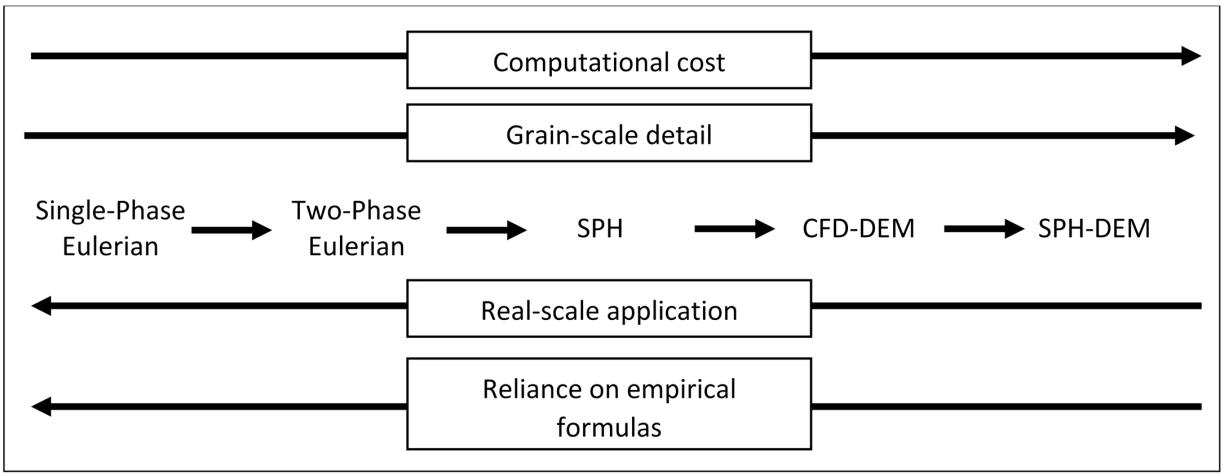


Figure 6. Qualitative positioning of single-phase Eulerian, two-phase Eulerian, SPH, CFD–DEM and SPH–DEM scour models along four key dimensions. Arrows indicate increasing levels of each dimension.

Table 1. Comparative overview of scour modelling methodologies.

	Single-Phase CFD	Two-Phase CFD	CFD–DEM	SPH	SPH–DEM
Fluid model	CFD/N-S	CFD/N-S	CFD/N-S	Lagrangian/N-S	Lagrangian/N-S
Sediment Model	Not explicit/ empirical formulas	CFD/N-S	Lagrangian/Newton's second law	Lagrangian/N-S	Lagrangian/Newton's second law
Limited to	• Dilute sediment transport [49] • Moderate flow velocities [49]	• Flow conditions comparable to those used to calibrate the adopted rheology	• Very-small-scale problems [110]	• Cases where turbulence–sediment coupling is not dominant [134]	• Very-small-scale problems • Cases where turbulence–sediment coupling is not dominant [134]

Table 1. *Cont.*

	Single-Phase CFD	Two-Phase CFD	CFD–DEM	SPH	SPH–DEM
Applications	• Engineering-scale assessments [34]	• Dense sediment transport [48] • Sheet-flow layers [49] • Strong sediment–turbulence coupling [82]	• Grain-scale mechanics [110] • Incipient-motion studies [25,54]	• Large deformations [134,139] • Free-surface dominated flows [134,139] • Reliable immobile-bed tracking [50]	• Grain-scale physics combined with large deformation [135] • Fluid–soil–structure interaction [135]

8.2. Applicability to Engineering Scour Problems

Given that each modelling approach is based on distinct assumptions and has different ranges of applicability, as outlined above, practical model selection should be guided by the specific engineering problem under consideration. Table 2 provides an application-specific ranking of the reviewed methods. Four categories are adopted: Preferred (P), where the method provides an appropriate balance between representation of the dominant physics, computational feasibility, and validation maturity; Suitable with limitations (S), where the method is applicable but important limitations related to physical assumptions, calibration, computational demand, or validation remain; Research-oriented (R), where the method provides valuable physical insight but is presently more appropriate for mechanism-focused or specialised studies than routine engineering prediction; and Not recommended (N), where key processes are not represented adequately or the method is presently impractical at the required scale. The table highlights that model suitability depends on the intended application, the required level of physical resolution, computational feasibility, and the flow and sediment conditions.

Table 2. Applicability ranking of modelling approaches to representative engineering scour problems. The ranking categories adopted are: Preferred (P), Suitable with limitations (S), Research-oriented (R), and Not recommended (N).

Engineering Scour Problem	Single-Phase CFD	Two-Phase CFD	CFD–DEM	SPH	SPH–DEM
Routine design screening and large-scale parametric studies.	**P**—Most practical where sediment feedback is limited.	**S**—Applicable where sediment feedback is important. Applicability depends on domain size and available calibration data.	**N**—Computationally impractical.	**S**—Low to medium suitability, depending on resolution requirements and validation evidence.	**N**—Computationally impractical.
Monopile or bridge-pier scour under steady current.	**P**—Suitable for preliminary and engineering-scale assessment when sediment feedback is limited.	**P**—High suitability where dense transport, live-bed behaviour, or bed failure is important.	**R**—Useful for grain-scale mechanisms.	**S**—Useful when large deformation or interface motion is central.	**R**—Useful for grain-scale mechanisms.
Wave-induced scour around offshore foundations.	**S**—Suitable where sediment feedback is limited and free-surface effects and sediment closures are appropriately calibrated.	**P**—High suitability for dense oscillatory transport and sediment-fluid feedback.	**R**—Useful for grain-scale mechanisms.	**P**—Useful for free-surface dominated cases.	**R**—Useful for grain-scale mechanisms.

Table 2. *Cont.*

Engineering Scour Problem	Single-Phase CFD	Two-Phase CFD	CFD–DEM	SPH	SPH–DEM
Pipeline scour onset and backfilling.	**S**—Practical for parametric and engineering-scale assessment. Suitable where sediment feedback is limited.	**P**—Highly suitable in such investigations.	**P**—Particularly useful for investigating scour-onset mechanisms at small scale.	**S**—Useful for large deformation and moving-bed cases.	**R**—Specialised grain-scale application with high computational cost.
Sheet flow and high-concentration transport.	**N**—Passive-sediment assumptions may become invalid.	**P**—Sediment concentration and granular stresses are resolved in a continuum sense.	**R**—Physically informative but restricted to small domains and durations.	**S**—Suitability depends on sediment formulation and stabilisation.	**N**—Computationally impractical, with no significant advantages over CFD–DEM for sheet-flow investigations.
Grain-scale mechanisms, incipient motion, and avalanching.	**N**—Particle contacts are not resolved explicitly.	**S**—Represented indirectly through continuum granular closures, which define its reliability.	**P**—Individual grains, contacts and particle forces are explicitly represented.	**S**—Useful for incipient-motion and deformation studies. Maturity restricts application as continuum SPH does not explicitly resolve real grains.	**R**—Explicit granular mechanics are represented, but current computational cost and maturity restrict application.
Free-surface representation, large bed deformations, and moving boundaries	**S**—Applicable with free-surface and moving-bed treatments, but less robust under severe deformation.	**S**—Physically robust but computationally demanding, especially with free-surface effects.	**N**—Not generally advantageous and high computational cost.	**P**—Mesh-free formulation is particularly advantageous for severe interface and bed deformation.	**N**—Requires large computational domains, rendering the simulation with DEM computationally prohibitive.
Sediment–fluid–structure interaction accounting for coupled structural motion or failure.	**N**—Conventional formulations normally assume fixed structures.	**N**—Conventional formulations normally assume fixed structures.	**N**—Conventional formulations normally assume fixed structures.	**S**—Moving structures can be accommodated in mesh-free formulations, subject to validation.	**R**—Particularly suited physically to coupled scour and structural motion, but restricted mainly to research-scale applications

8.3. Validation Maturity and Practical Implementation Considerations

In addition to physical suitability, the practical value of a modelling approach depends on the extent to which it has been validated and the level of confidence that can be assigned to its predictions. Table 3 summarises for each approach the typical validation data used, its current level of engineering maturity, and key considerations for practical application. The table highlights that validation maturity varies substantially across the reviewed methods and that greater physical detail does not necessarily translate into higher readiness for routine engineering use. It also indicates that practical implementation depends not only on model formulation, but also on calibration data, numerical resolution, closure assumptions, and the availability of appropriate experimental or field evidence.

Table 3. Validation maturity and key considerations for the practical application of each modelling method.

Method	Validation Data	Engineering Maturity	Key Considerations for Application
Single-Phase CFD	Laboratory flume tests measuring equilibrium scour depth, bed-profile evolution, and flow velocity fields.	Relatively mature for preliminary and large-scale engineering assessment.	Ensure that sediment concentrations remain sufficiently low, and that the selected transport and turbulence closures are validated for the flow regime.

Table 3. *Cont.*

Method	Validation Data	Engineering Maturity	Key Considerations for Application
Two-Phase CFD	Laboratory tests measuring equilibrium scour depth, bed-profile evolution, velocity profiles, and sediment-concentration profiles.	Increasing maturity for research and advanced design support.	Care is required to ensure that the simulated conditions are consistent with the calibration range of the adopted granular rheology, turbulence closure, and turbulence–sediment coupling models.
CFD–DEM	Laboratory tests measuring local scour, velocity profiles, and grain motion.	Medium maturity for grain-scale mechanism investigations. Very low maturity for routine design.	Particle size, contact parameters, drag law, CFD-cell-to-particle-size ratio, averaging assumptions, and DEM time step restrictions strongly influence both computational feasibility and result reliability. Direct full-scale engineering application is not currently practical.
SPH/SPH–DEM	Laboratory-scale tests measuring local scour in flume experiments, sediment motion induced by water flushing, dam-break, and free-surface motion.	Low maturity but promising for large deformation and free-surface dominated problems. Low maturity for routine design and strongly turbulent scour applications.	Careful selection of particle spacing, kernel treatment, pressure stabilisation, boundary treatment, and turbulence representation is required. Applications involving significant turbulence or field-scale domains require particular caution and further validation.

9. Remaining Challenges and Suggestions for Future Research

Despite substantial methodological progress, scalability remains a major constraint on the predictive reliability and practical use of numerical scour simulations. Single-phase Eulerian models are the most feasible for large-scale applications but cannot resolve key sediment–flow feedback mechanisms, whereas two-phase CFD, CFD–DEM, SPH, and SPH–DEM become computationally prohibitive for realistic three-dimensional geometries or long-duration events. Although DEM-informed upscaling functions and hybrid continuum–particle models are promising, they require further validation and generalisation. Validation in the reviewed literature remains largely based on laboratory data, while high-resolution field data suitable for detailed model validation remain comparatively scarce. This limits confidence in the transfer of numerical predictions from laboratory to field scale, particularly because Reynolds-number effects, sediment-to-fluid density ratios, and coherent turbulent structures may not be reproduced reliably in scaled experiments or coarsely resolved simulations.

Progress should therefore focus on improving model scalability, validation datasets, and the representation of the governing physical processes. From a numerical perspective, priority should be given to computationally efficient approaches capable of representing sediment–flow feedback at engineering scale. This includes improved morphodynamic formulations for single-phase models, validated upscaling strategies, and hybrid or multi-scale approaches that transfer information from particle-scale CFD–DEM simulations to continuum models without resolving individual sediment particles throughout the full computational domain. Further work should also examine hydrodynamic–morphodynamic

coupling strategies that reduce computational cost while maintaining numerical stability and sediment-mass conservation.

Turbulence modelling remains another major challenge. Existing RANS closures are predominantly calibrated for clear fluids, making their application to flows with dense suspended sediments questionable. While Reynolds-averaged approaches remain dominant in engineering applications, their inability to capture the unsteady vortex dynamics that drive local scour indicates the need for broader assessment and application of LES and hybrid RANS–LES approaches. These approaches are particularly relevant for scour dominated by horseshoe and wake vortices, but they remain too computationally demanding for routine use. Further research should therefore focus on developing and validating turbulence closures that account for sediment-induced damping, stratification, coherent vortical structures, and two-way coupling between turbulent fluctuations and sediment motion.

Sediment rheology also requires further development because continuum closures are often calibrated under narrow experimental conditions. Sediment stress closures should be extended to improve the representation of particle shape, grain-size distribution, and cohesion, while maintaining validity across wider sediment-concentration and mobility regimes. In CFD–DEM, further work is needed to improve the calibration and validation of contact laws and drag correlations, represent non-spherical and graded sediments more realistically, and address the computational restrictions associated with realistic particle numbers and grain-size distributions.

Laboratory datasets [10–13,147] provide valuable benchmarks, but they represent a narrow range of sediment types, flow regimes, and structural geometries. Experimental studies should move beyond validation based primarily on equilibrium scour depth. Laboratory programmes would benefit from simultaneous measurements of bed morphology, three-dimensional velocity and turbulence fields, suspended-sediment concentration, pore pressure, and, where feasible, individual grain motion. Particular attention should be given to clear-water and live-bed conditions, including high-concentration sheet-flow regimes, combined wave–current and transient loading, and representative structures such as monopiles, pile groups, pipelines, and caissons. Testing different structural configurations is important because they generate different flow-separation, vortex, and scour patterns, allowing assessment of whether numerical models remain reliable across structural geometries beyond those used for calibration and validation. Such datasets would allow validation not only of the final scour geometry but also of the hydrodynamic and sediment-transport mechanisms responsible for its development.

Field datasets, while capturing real-world variability, often lack the spatial and temporal resolution needed for detailed model validation. Long-duration in-field monitoring should combine repeated or continuous measurements of seabed evolution and scour-hole geometry with concurrent measurements of waves, currents, near-bed velocities, sediment concentrations, and relevant seabed properties. Event-resolved observations during storms and other energetic conditions are particularly important for assessing whether models calibrated against laboratory experiments can reproduce scour development, backfilling, and recovery under realistic environmental loading. The development of openly accessible benchmark datasets covering different sediment types, structural configurations, and hydrodynamic conditions would also enable more consistent comparison and validation of competing numerical approaches.

A further research need is the closer integration of scour prediction with geotechnical foundation-performance assessment. Increasing scour depth reduces foundation embedment and soil confinement and alters the soil resistance and failure mechanisms mobilised around the foundation [5,148,149]. Scour-induced soil loss may also reduce the extent of soil–foundation contact. More generally, Koronides et al. [150,151] have shown that soil–

foundation interface separation and gapping can significantly alter the dynamic response of soil–structure systems. However, bearing-capacity degradation cannot generally be related to scour depth alone, since it also depends on scour-hole geometry, soil properties, foundation configuration and loading conditions. Future studies should therefore couple evolving scour morphologies predicted by hydrodynamic–morphodynamic models with geotechnical analyses to establish validated relationships between scour development and the corresponding degradation of foundation capacity. Such coupling would also be valuable for assessing offshore foundations, for which the interaction between scour evolution and the modified soil–foundation load-transfer mechanism remains insufficiently characterised.

10. Conclusions

This review examined the principal numerical strategies used to simulate scour around coastal and offshore infrastructure, highlighting their underlying formulations, strengths, limitations, and practical applicability. The reviewed methods span a broad modelling spectrum, ranging from single-phase Eulerian models and two-phase Eulerian–Eulerian formulations to CFD–DEM coupling strategies and mesh-free SPH-based approaches. A distinguishing feature of the present review relative to previous review studies is the systematic comparison of these continuum, discrete, and mesh-free frameworks using common evaluation criteria. The comparative assessment has given emphasis on methods' engineering applicability, computational cost, validation maturity, physical fidelity, and ability to represent relevant seabed–fluid–structure interaction mechanisms. Overall, the most appropriate method depends on the engineering objective, the required level of physical detail, the sediment-transport regime, the prevailing flow conditions, the availability of validation data, and the computational demand. Model selection should also ensure consistency between the intended simulation conditions and the capability of the chosen method to represent key processes such as turbulence, sediment rheology, and sediment–flow feedback.

Based on the synthesis of the recent literature, the following key outcomes can be identified:

- Single-phase Eulerian CFD is the preferred approach for routine engineering screening, large-domain or long-duration simulations, and parametric studies where sediment concentrations remain sufficiently low for sediment–flow feedback to be neglected. Typical applications include preliminary assessment of monopile, bridge-pier, pipeline, and offshore-foundation scour under clear-water or weakly live-bed conditions. It is less appropriate where dense suspension, sheet flow, strong sediment–turbulence interaction, or momentary bed failure controls the response.
- Two-phase Eulerian–Eulerian CFD is more appropriate when dense sediment transport, sheet flow, granular stresses, or strong sediment–flow feedback are important. It is therefore particularly useful for advanced analysis of energetic current- and wave-induced scour. Its application requires appropriate validation of sediment rheology, interphase drag, and turbulence closures, and its computational demands make it less suitable for routine large-domain or long-duration simulations.
- CFD–DEM is most useful for mechanism-focused studies in which grain-scale behaviour is itself of interest, including incipient motion, particle contacts, avalanching, seepage-induced instability, and particle-scale sediment transport. It is presently impractical for direct field-scale or long-duration scour prediction because of the number of particles and small DEM time steps required. CFD–DEM should therefore primarily be regarded as a research and model-development tool that can inform continuum closures and reduced-order engineering models.

- SPH is particularly useful when large free-surface deformation, rapid bed evolution, sediment collapse, or moving boundaries are central to the problem and would create difficulties for grid-based methods. Examples include local or laboratory-scale problems involving strongly deforming fluid–sediment interfaces and transient wave loading. Its high computational demand, less mature turbulence treatments, and limited field-scale validation currently restrict its use for routine long-duration engineering prediction.
- SPH–DEM is most appropriate when the advantages of mesh-free free-surface modelling must be combined with explicit granular mechanics or structural motion, for example scour accompanied by displacement or tilting of a caisson. However, the combined particle-resolution and DEM requirements make it one of the most computationally demanding approaches considered. It should therefore presently be regarded primarily as a specialised research tool rather than a routine full-scale design method.

For present engineering practice, single-phase CFD therefore provides the most practical starting point when its underlying assumptions are satisfied, while two-phase CFD is justified when sediment–flow feedback becomes important. CFD–DEM, SPH, and SPH–DEM should be selected when the specific mechanisms they resolve are central to the analysis and when their restrictions on computational scale and validation are acceptable.

Future research should prioritise scalability, validation, and improved representation of the physical processes governing scour. This includes the development of computationally efficient approaches that can represent sediment–flow feedback and bed evolution at engineering scales, with particular emphasis on improved morphodynamic formulations for single-phase models and validated upscaling strategies. Further progress is also required in turbulence modelling for sediment-laden flows, particularly through closures that account for sediment-induced damping, stratification, coherent vortex structures, and two-way coupling between turbulent fluctuations and moving grains. In parallel, sediment rheology models need to incorporate more realistic representations of grain shape, grain-size distribution, and cohesion while extending their validity across broader sediment-concentration and mobility regimes. Experimental studies should move beyond validation based primarily on equilibrium scour depth and provide simultaneous measurements of bed evolution, flow and turbulence, sediment concentration, and, where feasible, grain motion and pore pressure. These laboratory datasets should be complemented by long-term, event-resolved field monitoring combining seabed morphology with concurrent measurements of waves, currents, sediment transport, and seabed conditions. Greater integration of numerical scour models with geotechnical foundation-response analyses is also needed to translate predicted scour development into consequences for structural performance. Together, these developments would improve the reliability and practical applicability of numerical scour prediction for the design and management of coastal and offshore infrastructure.

Author Contributions: Conceptualisation, M.K., T.O. and C.M.; formal analysis, M.K.; funding acquisition, M.K. and T.O.; investigation, M.K.; methodology, M.K., T.O. and C.M.; project administration, T.O.; resources, M.K., T.O. and C.M.; supervision, T.O.; validation, M.K., T.O. and C.M.; visualisation, M.K.; writing—original draft, M.K.; writing—review and editing, T.O. and C.M. All authors have read and agreed to the published version of the manuscript.

Funding: This research was funded by the Cyprus Ministry of Energy Commerce and Industry.

Data Availability Statement: No new data were created or analysed in this study. Data sharing is not applicable to this article.

Conflicts of Interest: The authors declare no conflicts of interest.

References

1. Pinto, F.; Rosa-Santos, P.; Lara, J.L.; Ramos, V. Scour near low-crested breakwaters: Review and technical challenges. *Appl. Ocean Res.* **2025**, *158*, 104582. [CrossRef]
2. Pizarro, A.; Manfreda, S.; Tubaldi, E. The science behind scour at bridge foundations: A review. *Water* **2020**, *12*, 374. [CrossRef]
3. Wardhana, K.; Hadipriono, F.C. Analysis of Recent Bridge Failures in the United States. *J. Perform. Constr. Facil.* **2003**, *17*, 144–150. [CrossRef]
4. Wei, W.; Malekjafarian, A.; Salauddin, M. Scour Protection Measures for Offshore Wind Turbines: A Systematic Literature Review on Recent Developments. *Energies* **2024**, *17*, 1068. [CrossRef]
5. Ciancimino, A.; Anastasopoulos, I.; Foti, S.; Gajo, A. Numerical modelling of the effects of foundation scour on the response of a bridge pier. *Acta Geotech.* **2022**, *17*, 3697–3717. [CrossRef]
6. Kim, Y.-J.; Lim, J.S.; Kim, H.J.; Choi, S.-W. A comprehensive review of foundation designs for fixed offshore wind turbines. *Int. J. Nav. Archit. Ocean Eng.* **2025**, *17*, 100643. [CrossRef]
7. Yu, S.Y.; Choi, H.S.; Lee, S.K.; Park, K.S.; Kim, D.-K. Nonlinear soil parameter effects on dynamic embedment of offshore pipeline on soft clay. *Int. J. Nav. Archit. Ocean Eng.* **2015**, *7*, 227–243. [CrossRef]
8. Duan, B.; Wang, D.; Qin, C.; Duan, L. Local Scour Around Marine Structures: A Comprehensive Review of Influencing Factors, Prediction Methods, and Future Directions. *Buildings* **2025**, *15*, 2125. [CrossRef]
9. Sumer, B.M.; Fredsøe, J. *The Mechanics of Scour in the Marine Environment, Advanced Series on Ocean Engineering*; World Scientific Publishing Company: Singapore, 2002. [CrossRef]
10. Dey, S.; Sumer, B.M.; Fredsøe, J. Control of Scour at Vertical Circular Piles under Waves and Current. *J. Hydraul. Eng.* **2006**, *132*, 270–279. [CrossRef]
11. Roulund, A.; Sumer, B.M.; Fredsøe, J.; Michelsen, J. Numerical and experimental investigation of flow and scour around a circular pile. *J. Fluid Mech.* **2005**, *534*, 351–401. [CrossRef]
12. Sumer, B.M.; Sen, M.B.; Karagali, I.; Ceren, B.; Fredsøe, J.; Sottile, M.; Zilioli, L.; Fuhrman, D.R. Flow and sediment transport induced by a plunging solitary wave. *J. Geophys. Res. Ocean.* **2011**, *116*, C01008. [CrossRef]
13. Sumer, B.M.; Fredsøe, J. Experimental study of 2D scour and its protection at a rubble-mound breakwater. *Coast. Eng.* **2000**, *40*, 59–87. [CrossRef]
14. Conley, D.C.; Inman, D.L. Field observations of the fluid-granular boundary layer under near-breaking waves. *J. Geophys. Res.* **1992**, *97*, 9631–9643. [CrossRef]
15. Foster, D.L.; Bowen, A.J.; Holman, R.A.; Natoo, P. Field evidence of pressure gradient induced incipient motion. *J. Geophys. Res. Oceans* **2006**, *111*, 9631–9643. [CrossRef]
16. Gowthaman, R.; Sanil Kumar, V.; Dwarakish, G.S.; Shanas, P.R.; Jena, B.K.; Singh, J. Nearshore waves and longshore sediment transport along Rameshwaram island off the east coast of India. *Int. J. Nav. Archit. Ocean Eng.* **2015**, *7*, 939–950. [CrossRef]
17. Tang, Y.; Wu, Z.; Sneed, L.H. A critical review of bridge scour monitoring methods. *J. Civ. Struct. Health Monit.* **2025**, *15*, 2679–2703. [CrossRef]
18. Zhao, M. A Review on Recent Development of Numerical Modelling of Local Scour around Hydraulic and Marine Structures. *J. Mar. Sci. Eng.* **2022**, *10*, 1139. [CrossRef]
19. Yang, Q.; Hu, R.; Yu, P.; Zhang, P.; Xu, Z.; Xu, M. Local scour mechanisms and prediction methods around offshore wind turbine foundations: Insights and future directions. *J. Ocean Univ. China* **2024**, *23*, 1248–1262. [CrossRef]
20. Dinku, N.; Bao, T.; Cui, J.; Song, X.; Su, L.; Ding, X. A Review on Numerical Modelling of Scour Around Offshore Wind Turbine. *Arch. Comput. Methods Eng.* **2026**, 1–45. [CrossRef]
21. Guta, H.; Hurther, D.; Chauchat, J. Bed-load and Concentration Effects on Turbulent Suspension Properties in Heavy Particle Sheet Flows. *J. Hydraul. Eng.* **2022**, *148*, 04022012. [CrossRef]
22. Soulsby, R. *Dynamics of Marine Sands: A Manual for Practical Applications*; Thomas Telford Publications: London, UK, 1997.
23. Soulsby, R.L.; Whitehouse, R.J.S. Threshold of Sediment Motion in Coastal Environments. In *Pacific Coasts and Ports' 97: Proceedings of the 13th Australasian Coastal and Ocean Engineering Conference and the 6th Australasian Port and Harbour Conference*; Centre for Advanced Engineering, University of Canterbury, Christchurch: Christchurch, New Zealand, 1997; pp. 145–150.
24. Liang, D.; Huang, J.; Zhang, J.; Shi, S.; Zhu, N.; Chen, J. Three-Dimensional Simulations of Scour around Pipelines of Finite Lengths. *J. Mar. Sci. Eng.* **2022**, *10*, 106. [CrossRef]
25. Ma, H.; Zhang, S.; Li, B.; Huang, W. Local scour around the monopile based on the CFD-DEM method: Experimental and numerical study. *Comput. Geotech.* **2024**, *168*, 106117. [CrossRef]
26. Keetels, G.H.; Chauchat, J.; Breugem, W.-P. Role of turbulent kinetic energy modulation by particle-fluid interaction in sediment pick-up. *J. Fluid Mech.* **2023**, *955*, A37. [CrossRef]
27. Guo, Z.; Jeng, D.-S.; Zhao, H.; Guo, W.; Wang, L. Effect of seepage flow on sediment incipient motion around a free spanning pipeline. *Coast. Eng.* **2019**, *143*, 50–62. [CrossRef]

28. Zhai, H.; Jeng, D.-S.; Guo, Z. The role of 2D seepage on sediment incipient motion around a pipeline. *J. Mar. Sci. Eng.* **2021**, *9*, 580. [CrossRef]
29. Zhai, H.; Jeng, D.-S. Impacts of wave-induced seabed response on local scour around a pipeline: PORO–FSSI–SCOUR–FOAM. *Coast. Eng.* **2024**, *187*, 104424. [CrossRef]
30. Zhai, H.; Jeng, D.-S.; Guo, Z.; Sui, T. Modified Shields number for sediment incipient motion around a pile with impact of three-dimensional seepage in a porous seabed. *Appl. Ocean Res.* **2021**, *117*, 102896. [CrossRef]
31. Hu, Z.; Li, Y.P. Full-scale tsunami-induced scour around a circular pile with three-dimensional seepage. *Coast. Eng.* **2025**, *197*, 104676. [CrossRef]
32. Sumer, B.M.; Christiansen, N.; Fredsøe, J. The horseshoe vortex and vortex shedding around a vertical wall-mounted cylinder exposed to waves. *J. Fluid Mech.* **1997**, *332*, 41–70. [CrossRef]
33. Sumer, B.M.; Fredsøe, J. Wave scour around a large vertical circular cylinder. *J. Waterw. Port. Coast. Ocean Eng.* **2001**, *127*, 125–134. [CrossRef]
34. Ahmad, N.; Kamath, A.; Bihs, H. 3D numerical modelling of scour around a jacket structure with dynamic free surface capturing. *Ocean Eng.* **2020**, *200*, 107104. [CrossRef]
35. Lancaster, O.; Cossu, R.; Wilson, M.; Baldock, T.E. A 3D numerical and experimental parametric study of wave-induced scour around large bluff body structures. *Ocean Eng.* **2022**, *266*, 112766. [CrossRef]
36. Tabasi, M.; Mitsui, J.; Suzuki, T.; Kubota, S.-I.; Tanaka, M. Investigation of morphological changes around breakwaters with different wave-dissipating concrete blocks using physical and numerical models. *Coast. Eng. J.* **2025**, *67*, 335–349. [CrossRef]
37. Oliveto, G.; Hager, W.H. Temporal Evolution of Clear-Water Pier and Abutment Scour. *J. Hydraul. Eng.* **2002**, *128*, 811–820. [CrossRef]
38. Matsuo, D.; Sakaue, A.; Uchida, T. Development of an acceleration method for sediment transport analysis with suspended load and bed-load in an integrated river channel and coastal region. *Coast. Eng. J.* **2025**, *67*, 146–161. [CrossRef]
39. Ahmad, N.; Bihs, H.; Myrhaug, D.; Kamath, A.; Arntsen, Ø.A. Three-dimensional numerical modelling of wave-induced scour around piles in a side-by-side arrangement. *Coast. Eng.* **2018**, *138*, 132–151. [CrossRef]
40. Song, Y.; Xu, Y.; Ismail, H.; Liu, X. Scour modeling based on immersed boundary method: A pathway to practical use of three-dimensional scour models. *Coast. Eng.* **2022**, *171*, 104037. [CrossRef]
41. Cao, Z.; Day, R.; Egashira, S. Coupled and decoupled numerical modeling of flow and morphological evolution in alluvial rivers. *J. Hydraul. Eng.* **2002**, *128*, 306–321. [CrossRef]
42. Liu, X.; Beljadid, A. A coupled numerical model for water flow, sediment transport and bed erosion. *Comput. Fluids* **2017**, *154*, 273–284. [CrossRef]
43. Callaghan, D.P.; Saint-Cast, F.; Nielsen, P.; Baldock, T.E. Numerical solutions of the sediment conservation law; a review and improved formulation for coastal morphological modelling. *Coast. Eng.* **2006**, *53*, 557–571. [CrossRef]
44. Liu, Y.; Huang, M.; Yu, J. Three-dimensional numerical analysis of local scour around inclined twin piles with varying current directions. *Ocean Eng.* **2025**, *335*, 121631. [CrossRef]
45. Nagel, T.; Chauchat, J.; Bonamy, C.; Liu, X.; Cheng, Z.; Hsu, T.-J. Three-dimensional scour simulations with a two-phase flow model. *Adv. Water Resour.* **2020**, *138*, 103544. [CrossRef]
46. Yu, X.; Fuhrman, D.R.; Shao, Y. Improved immersed boundary/wall modeling method for RANS solver coupled with wall functions: Application to Cartesian grid systems. *Eng. Appl. Comput. Fluid Mech.* **2025**, *19*, 2486657. [CrossRef]
47. Jazaeri, S.A.; Nistor, I.; Mohammadian, A.; Liu, X. A critical review on the tsunami-induced scour around structures. *Coast. Eng. J.* **2024**, *66*, 563–590. [CrossRef]
48. Cheng, Z.; Hsu, T.-J.; Calantoni, J. SedFoam: A multi-dimensional Eulerian two-phase model for sediment transport and its application to momentary bed failure. *Coast. Eng.* **2017**, *119*, 32–50. [CrossRef]
49. Chauchat, J.; Cheng, Z.; Nagel, T.; Bonamy, C.; Hsu, T.-J. SedFoam-2.0: A 3-D two-phase flow numerical model for sediment transport. *Geosci. Model Dev.* **2017**, *10*, 4367–4392. [CrossRef]
50. Zhang, R.; Xiong, W.; Gao, Y. A meshless model for three-dimensional direct numerical simulation of local scour around cylinder bridge foundation. *Ocean Eng.* **2024**, *312*, 119220. [CrossRef]
51. Biao, L.; Wen-Gang, Q.; Yifa, W.; Fu-Ping, G.; Shun-Yi, W. Scour-induced unloading effects on lateral response of large–diameter monopiles in dense sand. *Comput. Geotech.* **2024**, *174*, 106635. [CrossRef]
52. Han, Z.; Ding, H.; Yan, H.; Zeng, C.; Li, C.; Xie, W.; Fu, B.; Li, Y. Investigating the bearing performance of the foundation under the combined effects of flood scouring and soaking. *Sci. Rep.* **2023**, *13*, 22823. [CrossRef]
53. Wang, J.; Zhao, T.; Zhu, J.; Gou, H. Simulation test of continuous rigid frame railway bridge under flood scouring. *Structures* **2024**, *66*, 106893. [CrossRef]
54. Zhang, S.; Li, B.; Ma, H. Numerical investigation of scour around the monopile using CFD-DEM coupling method. *Coast. Eng.* **2023**, *183*, 104334. [CrossRef]

55. Ikani, N.; Pu, J.H.; Soori, S. Flow Pattern and Turbulent Kinetic Energy Analysis Around Tandem Piers: Insights from k-ε Modelling and Acoustic Doppler Velocimetry Measurements. *Water* **2025**, *17*, 1100. [CrossRef]
56. Yu, T.; Wang, Y.; Tong, X.; Yan, Z.; Wang, D.; Zhang, C. Numerical and experimental study on local scour in front of OWC-BWS under waves. *Mar. Georesources Geotechnol.* **2025**, *43*, 694–704. [CrossRef]
57. Dhamelia, V.; Zhao, M.; Hu, P.; Palmer, H. Numerical investigation of local scour around a 2-degree of freedom vibrating subsea pipeline in steady flow under sagging condition. *Ocean Eng.* **2025**, *315*, 119890. [CrossRef]
58. Dhamelia, V.; Zhao, M.; Hu, P. Numerical investigation of local scour around a vertically vibrating subsea pipeline under steady flow. *Ocean Eng.* **2023**, *285*, 115437. [CrossRef]
59. Launder, B.E.; Spalding, D.B. The numerical computation of turbulent flows. *Comput. Methods Appl. Mech. Eng.* **1974**, *3*, 269–289. [CrossRef]
60. Menter, F. Zonal two equation k-ω turbulence models for aerodynamic flows. In Proceedings of the 24th Fluid Dynamics Conference, Orlando, FL, USA, 6–9 July 1993.
61. Smagorinsky, J. General circulation experiments with the primitive equations: I. The basic experiment. *Mon. Weather Rev.* **1963**, *91*, 99–164.
62. Meyer-Peter, E.; Muller, R. Formulas for bed-load transport. In Proceedings of the 2nd Meeting of the International Association of Hydraulic and Structural Research, Stockholm, Sweden, 7–9 June 1948; pp. 34–64.
63. Van Rijn, L.C. Sediment transport, part I: Bed load transport. *J. Hydraul. Eng.* **1984**, *110*, 1431–1456. [CrossRef]
64. Engelund, F.; Fredsee, J. A Sediment Transport Model for Straight Alluvial Channels. *Hydrol. Res.* **1976**, *7*, 293–306. [CrossRef]
65. Dixen, M.; Sumer, B.M.; Fredsøe, J. Numerical and experimental investigation of flow and scour around a half-buried sphere. *Coast. Eng.* **2013**, *73*, 84–105. [CrossRef]
66. Baykal, C.; Sumer, B.M.; Fuhrman, D.R.; Jacobsen, N.G.; Fredsoe, J. Numerical investigation of flow and scour around a vertical circular cylinder. *Philos. Trans. R. Soc. A Math. Phys. Eng. Sci.* **2015**, *373*, 20140104. [CrossRef]
67. Dentale, F.; Reale, F.; Di Leo, A.; Carratelli, E.P. A CFD approach to rubble mound breakwater design. *Int. J. Nav. Archit. Ocean Eng.* **2018**, *10*, 644–650. [CrossRef]
68. Osher, S.; Sethian, J.A. Fronts Propagating with Curvature-Dependent Speed: Algorithms Based on Hamilton-Jacobi Formulations. *J. Comput. Phys.* **1988**, *79*, 12–49. [CrossRef]
69. Peng, D.; Merriman, B.; Osher, S.; Zhao, H.; Kang, M. A PDE-Based Fast Local Level Set Method 1. *J. Comput. Phys.* **1999**, *155*, 410–438. [CrossRef]
70. Sussman, M.; Puckett, E.G. A Coupled Level Set and Volume-of-Fluid Method for Computing 3D and Axisymmetric Incompressible Two-Phase Flows. *J. Comput. Phys.* **2000**, *162*, 301–337. [CrossRef]
71. Wu, W.; Rodi, W.; Wenka, T. 3D Numerical modeling of flow and sediment transport in open channels. *J. Hydraul. Eng.* **2000**, *126*, 4–15. [CrossRef]
72. van Rijn, L.C. Mathematical modeling of suspended sediment in nonuniform flows. *J. Hydraul. Eng.* **1986**, *112*, 433–455. [CrossRef]
73. Burkow, M.; Griebel, M. A full three dimensional numerical simulation of the sediment transport and the scouring at a rectangular obstacle. *Comput. Fluids* **2016**, *125*, 1–10. [CrossRef]
74. Baykal, C.; Sumer, B.M.; Fuhrman, D.R.; Jacobsen, N.G.; Fredsøe, J. Numerical simulation of scour and backfilling processes around a circular pile in waves. *Coast. Eng.* **2017**, *122*, 87–107. [CrossRef]
75. Jasak, H.; Tukovic, Z. Automatic mesh motion for the unstructured finite volume method. *Trans. FAMENA* **2006**, *30*, 1–20.
76. Zhao, M.; Cheng, L.; Zang, Z. Experimental and numerical investigation of local scour around a submerged vertical circular cylinder in steady currents. *Coast. Eng.* **2010**, *57*, 709–721. [CrossRef]
77. Berthelsen, P.A.; Faltinsen, O.M. A local directional ghost cell approach for incompressible viscous flow problems with irregular boundaries. *J. Comput. Phys.* **2008**, *227*, 4354–4397. [CrossRef]
78. Marella, S.; Krishnan, S.; Liu, H.; Udaykumar, H.S. Sharp interface Cartesian grid method I: An easily implemented technique for 3D moving boundary computations. *J. Comput. Phys.* **2005**, *210*, 1–31. [CrossRef]
79. Tseng, Y.H.; Ferziger, J.H. A ghost-cell immersed boundary method for flow in complex geometry. *J. Comput. Phys.* **2003**, *192*, 593–623. [CrossRef]
80. Udaykumar, H.S.; Mittal, R.; Shyy, W. Computation of Solid–Liquid Phase Fronts in the Sharp Interface Limit on Fixed Grids. *J. Comput. Phys.* **1999**, *153*, 535–574. [CrossRef]
81. Gilletta, A.; Bonamy, C.; Robert, M.; Chauchat, J. Assessment of hybrid RANS/LES models for the prediction of the flow and scour around a wall-mounted cylinder. *Adv. Water Resour.* **2025**, *199*, 104934. [CrossRef]
82. Mathieu, A.; Kim, Y.; Hsu, T.-J.; Bonamy, C.; Chauchat, J. sedInterFoam 1.0: A three-phase numerical model for sediment transport applications with free surfaces. *Geosci. Model Dev.* **2025**, *18*, 1561–1573. [CrossRef]
83. Drew, D.A. *Mathematical Modeling of Two-Phase Flow*; Technical Summary Report No. 2343; Mathematics Research Center, University of Wisconsin–Madison: Madison, WI, USA, 1982.

84. Jackson, R. Locally averaged equations of motion for a mixture of identical spherical particles and a Newtonian fluid. *Chem. Eng. Sci.* **1997**, *52*, 2457–2469. [CrossRef]
85. Liu, H.; Wu, W.; Jiang, G.; El Naggar, M.H.; Mei, G.; Liang, R. Influence of soil plug effect on the vertical dynamic response of large diameter pipe piles. *Ocean Eng.* **2018**, *157*, 13–25. [CrossRef]
86. Amoudry, L.; Hsu, T.J.; Liu, P.L.F. Two-phase model for sand transport in sheet flow regime. *J. Geophys. Res. Ocean.* **2008**, *113*, C03011. [CrossRef]
87. Hsu, T.J.; Liu, P.L.F. Toward modeling turbulent suspension of sand in the nearshore. *J. Geophys. Res. Ocean.* **2004**, *109*, C06018. [CrossRef]
88. Cassar, C.; Nicolas, M.; Pouliquen, O. Submarine granular flows down inclined planes. *Phys. Fluids* **2005**, *17*, 103301. [CrossRef]
89. Jenkins, J.T.; Savage, S.B. A theory for the rapid flow of identical, smooth, nearly elastic, spherical particles. *J. Fluid Mech.* **1983**, *130*, 187–202. [CrossRef]
90. Johnson, P.C.; Jackson, R. Frictional-collisional constitutive relations for granular materials, with application to plane shearing. *J. Fluid Mech.* **1987**, *176*, 67–93. [CrossRef]
91. Ding, J.; Gidaspow, D. A Bubbling Fluidization Model Using Kinetic Theory of Granular Flow. *AIChE J.* **1990**, *36*, 523–538. [CrossRef]
92. Torquato, S. Nearest-neighbor statistics for packings of hard spheres and disks. *Phys. Rev. E* **1995**, *51*, 3170–3182. [CrossRef]
93. Gidaspow, D. *Multiphase Flow and Fluidization: Continuum and Kinetic Theory Descriptions*; Academic Press: Cambridge, MA, USA, 1994.
94. Hsu, T.-J.; Jenkins, J.T.; Liu, P.L.-F. On two-phase sediment transport: Sheet flow of massive particles. *Proc. R. Soc. A Math. Phys. Eng. Sci. R. Soc.* **2004**, *460*, 2223–2250. [CrossRef]
95. Jenkins, J.T.; Richman, M.W. Grad's 13-Moment System for a Dense Gas of Inelastic Spheres. *Arch. Ration. Mech. Anal.* **1985**, *87*, 355–377. [CrossRef]
96. Jop, P.; Forterre, Y.; Pouliquen, O. A constitutive law for dense granular flows. *Nature* **2006**, *441*, 727–730. [CrossRef]
97. Jop, P.; Forterre, Y.; Pouliquen, O. Crucial role of sidewalls in granular surface flows: Consequences for the rheology. *J. Fluid Mech.* **2005**, *541*, 167–192. [CrossRef]
98. Forterre, Y.; Pouliquen, O. Flows of Dense Granular Media. *Annu. Rev. Fluid Mech.* **2008**, *40*, 1–24. [CrossRef]
99. Kamrin, K.; Koval, G. Nonlocal Constitutive Relation for Steady Granular Flow. *Phys. Rev. Lett.* **2012**, *108*, 178301. [CrossRef]
100. Henann, D.L.; Kamrin, K. A predictive, size-dependent continuum model for dense granular flows. *Proc. Natl. Acad. Sci. USA* **2013**, *110*, 6730–6735. [CrossRef]
101. Zhang, Q.; Kamrin, K. Microscopic Description of the Granular Fluidity Field in Nonlocal Flow Modeling. *Phys. Rev. Lett.* **2017**, *118*, 058001. [CrossRef]
102. Boyer, F.; Guazzelli, É.; Pouliquen, O. Unifying suspension and granular rheology. *Phys. Rev. Lett.* **2011**, *107*, 188301. [CrossRef]
103. Khamseh, S.; Roux, J.N.; Chevoir, F. Flow of wet granular materials: A numerical study. *Phys. Rev. E* **2015**, *92*, 022201. [CrossRef]
104. Rognon, P.G.; Roux, J.-N.; Naaim, M.; Chevoir, F. Dense flows of cohesive granular materials. *J. Fluid Mech.* **2008**, *596*, 21–47. [CrossRef]
105. Blatny, L.; Gray, J.M.; Gaume, J. A critical state μ(I)-rheology model for cohesive granular flows. *J. Fluid Mech.* **2024**, *997*, A67. [CrossRef]
106. Maurin, R.; Chauchat, J.; Frey, P. Dense granular flow rheology in turbulent bed-load transport. *J. Fluid Mech.* **2016**, *804*, 490–512. [CrossRef]
107. Amoudry, L.; Hsu, T.-J.; Liu, P.L.-F. Schmidt number and near-bed boundary condition effects on a two-phase dilute sediment transport model. *J. Geophys. Res. Ocean.* **2005**, *110*, C09003. [CrossRef]
108. van Rijn, L.C. Sediment Transport, Part II: Suspended Load Transport. *J. Hydraul. Eng.* **1984**, *110*, 1613–1641. [CrossRef]
109. Chauchat, J.; Guillou, S. On turbulence closures for two-phase sediment-laden flow models. *J. Geophys. Res. Ocean.* **2008**, *113*, C11017. [CrossRef]
110. Yazdanfar, Z.; Lester, D.; Robert, D.; Setunge, S. A novel CFD-DEM upscaling method for prediction of scour under live-bed conditions. *Ocean Eng.* **2021**, *220*, 108442. [CrossRef]
111. Menter, F.R. Two-equation eddy-viscosity turbulence models for engineering applications. *AIAA J.* **1994**, *32*, 1598–1605. [CrossRef]
112. Nguyen, T.H.T.; Park, S.; Jang, D.; Ahn, J. Evaluation of Three-Dimensional Environmental Hydraulic Modeling in Scour Hole. *Appl. Sci.* **2022**, *12*, 4032. [CrossRef]
113. Jha, S.K.; Bombardelli, F.A. Two-phase modeling of turbulence in dilute sediment-laden, open-channel flows. *Environ. Fluid Mech.* **2009**, *9*, 237–266. [CrossRef]
114. Wilcox, D.C. Reassessment of the scale-determining equation for advanced turbulence models. *AIAA J.* **1988**, *26*, 1299–1310. [CrossRef]
115. Amoudry, L.O. Extension of k-ω turbulence closure to two-phase sediment transport modelling: Application to oscillatory sheet flows. *Adv. Water Resour.* **2014**, *72*, 110–121. [CrossRef]

116. Jenkins, J.T.; Hanes, D.M. Collisional sheet flows of sediment driven by a turbulent fluid. *J. Fluid Mech.* **1998**, *370*, 29–52. [CrossRef]
117. Revil-Baudard, T.; Chauchat, J. A two-phase model for sheet flow regime based on dense granular flow rheology. *J. Geophys. Res. Ocean.* **2013**, *118*, 619–634. [CrossRef]
118. Tafarojnoruz, A.; Lauria, A. Large eddy simulation of the turbulent flow field around a submerged pile within a scour hole under current condition. *Coast. Eng. J.* **2020**, *62*, 489–503. [CrossRef]
119. Gritskevich, M.S.; Garbaruk, A.V.; Schütze, J.; Menter, F.R. Development of DDES and IDDES formulations for the k-ω shear stress transport model. *Flow Turbul. Combust.* **2012**, *88*, 431–449. [CrossRef]
120. Menter, F.R.; Egorov, Y. The scale-adaptive simulation method for unsteady turbulent flow predictions. part 1: Theory and model description. *Flow Turbul. Combust.* **2010**, *85*, 113–138. [CrossRef]
121. Salimi-Tarazouj, A.; Hsu, T.J.; Traykovski, P.; Chauchat, J. Investigating wave shape effect on sediment transport over migrating ripples using an eulerian two-phase model. *Coast. Eng.* **2024**, *189*, 104470. [CrossRef]
122. Mathieu, A.; Chauchat, J.; Bonamy, C.; Nagel, T. Two-phase flow simulation of tunnel and lee-wake erosion of scour below a submarine pipeline. *Water* **2019**, *11*, 1727. [CrossRef]
123. Tsai, B.; Mathieu, A.; Montellà, E.P.; Hsu, T.J.; Chauchat, J. An Eulerian two-phase flow model investigation on scour onset and backfill of a 2D pipeline. *Eur. J. Mech. B/Fluids* **2022**, *91*, 10–26. [CrossRef]
124. Velioglu Sogut, D.; Sogut, E.; Farhadzadeh, A.; Hsu, T.-J. Non-Equilibrium Scour Evolution around an Emerged Structure Exposed to a Transient Wave. *J. Mar. Sci. Eng.* **2024**, *12*, 946. [CrossRef]
125. Zhang, R.; Xiong, W.; Ma, X.; Cai, C.S. Progressive bridge collapse analysis under both scour and floods by coupling simulation in structural and hydraulic fields. Part I: Numerical solver. *Ocean Eng.* **2023**, *273*, 113849. [CrossRef]
126. Rhie, C.M.; Chow, W.L. Numerical study of the turbulent flow past an airfoil with trailing edge separation. *AIAA J.* **1983**, *21*, 1525–1532. [CrossRef]
127. Holzmann, T. *Mathematics, Numerics, Derivations and OpenFOAM®*; Holzmann CFD: Leoben, Austria, 2016.
128. Mindlin, R.D.; Deresiewicz, H. Elastic Spheres in Contact Under Varying Oblique Forces. *J. Appl. Mech.* **1953**, *20*, 327–344. [CrossRef]
129. Goniva, C.; Kloss, C.; Deen, N.G.; Kuipers, J.A.M.; Pirker, S. Influence of rolling friction on single spout fluidized bed simulation. *Particuology* **2012**, *10*, 582–591. [CrossRef]
130. Hu, D.; Tang, W.; Sun, L.; Li, F.; Ji, X.; Duan, Z. Numerical simulation of local scour around two pipelines in tandem using CFD–DEM method. *Appl. Ocean Res.* **2019**, *93*, 101968. [CrossRef]
131. Takabatake, K.; Mori, Y.; Khinast, J.G.; Sakai, M. Numerical investigation of a coarse-grain discrete element method in solid mixing in a spouted bed. *Chem. Eng. J.* **2018**, *346*, 416–426. [CrossRef]
132. Adesina, P.; O'Sullivan, C.; Wang, T. Understanding the interplay between particle shape, grading and sample density on the behaviour of granular assemblies: A DEM approach. *Granul. Matter* **2024**, *26*, 14. [CrossRef]
133. Gingold, R.A.; Monaghan, J.J. Smoothed particle hydrodynamics: Theory and application to non-spherical stars. *Mon. Not. R. Astron. Soc.* **1977**, *181*, 375–389. [CrossRef]
134. Wang, D.; Shao, S.; Li, S.; Shi, Y.; Arikawa, T.; Zhang, H. 3D ISPH erosion model for flow passing a vertical cylinder. *J. Fluids Struct.* **2018**, *78*, 374–399. [CrossRef]
135. Iwamoto, T.; Nakase, H.; Nishiura, D.; Sakaguchi, H.; Miyamoto, J.; Tsurugasaki, K.; Kiyono, J. Application of SPH-DEM coupled method to failure simulation of a caisson type composite breakwater during a tsunami. *Soil Dyn. Earthq. Eng.* **2019**, *127*, 105806. [CrossRef]
136. Yeganeh-Bakhtiary, A.; Houshangi, H.; Abolfathi, S. Lagrangian two-phase flow modeling of scour in front of vertical breakwater. *Coast. Eng. J.* **2020**, *62*, 252–266. [CrossRef]
137. Zhang, R.; Xiong, W.; Ma, X.; Cai, C.S. Mesh-free SPH modelling of sediment scouring and flushing considering grains transport and transformation. *Eng. Appl. Comput. Fluid Mech.* **2024**, *18*, 2367510. [CrossRef]
138. Lind, S.J.; Xu, R.; Stansby, P.K.; Rogers, B.D. Incompressible smoothed particle hydrodynamics for free-surface flows: A generalised diffusion-based algorithm for stability and validations for impulsive flows and propagating waves. *J. Comput. Phys.* **2012**, *231*, 1499–1523. [CrossRef]
139. Wang, Z.B.; Chen, R.; Wang, H.; Liao, Q.; Zhu, X.; Li, S.Z. An overview of smoothed particle hydrodynamics for simulating multiphase flow. *Appl. Math. Model* **2016**, *40*, 9625–9655. [CrossRef]
140. Antuono, M.; Colagrossi, A.; Marrone, S.; Molteni, D. Free-surface flows solved by means of SPH schemes with numerical diffusive terms. *Comput. Phys. Commun.* **2010**, *181*, 532–549. [CrossRef]
141. Fourtakas, G.; Rogers, B.D. Modelling multi-phase liquid-sediment scour and resuspension induced by rapid flows using Smoothed Particle Hydrodynamics (SPH) accelerated with a Graphics Processing Unit (GPU). *Adv. Water Resour.* **2016**, *92*, 186–199. [CrossRef]
142. Bui, H.H.; Fukagawa, R.; Sako, K.; Wells, J.C. Slope stability analysis and discontinuous slope failure simulation by elasto-plastic smoothed particle hydrodynamics (SPH). *Géotechnique* **2011**, *61*, 565–574. [CrossRef]

143. Zubeldia, E.H.; Fourtakas, G.; Rogers, B.D.; Farias, M.M. Multi-phase SPH model for simulation of erosion and scouring by means of the shields and Drucker–Prager criteria. *Adv. Water Resour.* **2018**, *117*, 98–114. [CrossRef]
144. Vand, V. Viscosity of Solutions and Suspensions. *I. Theory. J. Phys. Chem.* **1948**, *52*, 277–299. [CrossRef]
145. Dey, S. Threshold of sediment motion on combined transverse and longitudinal sloping beds. *J. Hydraul. Res.* **2003**, *41*, 405–415. [CrossRef]
146. Wu, H.; Wang, J.; Wang, C.; Wang, J.H. Soil-Water-Structure Interaction Algorithm in Smoothed Particle Hydrodynamics (SPH) with Application to Deep-Penetrating Problems. *Int. J. Comput. Methods* **2020**, *17*, 1850135. [CrossRef]
147. Sumer, B.M.; Fredsøe, J.; Christiansen, N. Scour around vertical pile in waves. *J. Waterw. Port. Coast. Ocean Eng.* **1992**, *118*, 15–31. [CrossRef]
148. Guo, X.; Liu, J.; Yi, P.; Feng, X.; Han, C. Effects of local scour on failure envelopes of offshore monopiles and caissons. *Appl. Ocean Res.* **2022**, *118*, 103007. [CrossRef]
149. Menéndez-Vicente, C.; López-Querol, S.; Bhattacharya, S.; Simons, R. Numerical study on the effects of scour on monopile foundations for Offshore Wind Turbines: The case of Robin Rigg wind farm. *Soil Dyn. Earthq. Eng.* **2023**, *167*, 107803. [CrossRef]
150. Koronides, M.; Kontoe, S.; Zdravković, L.; Vratsikidis, A.; Pitilakis, D. Numerical simulation of SSI free and forced vibration experiments on real scale structures of different stiffness. *Soil Dyn. Earthq. Eng.* **2023**, *175*, 108232. [CrossRef]
151. Koronides, M.; Kontoe, S.; Zdravković, L.; Vratsikidis, A.; Pitilakis, D. Experimental and numerical investigation of soil-foundation interface nonlinearity under dynamic loading. *Soil Dyn. Earthq. Eng.* **2026**, *200*, 109897. [CrossRef]

Disclaimer/Publisher's Note: The statements, opinions and data contained in all publications are solely those of the individual author(s) and contributor(s) and not of MDPI and/or the editor(s). MDPI and/or the editor(s) disclaim responsibility for any injury to people or property resulting from any ideas, methods, instructions or products referred to in the content.